J Neurophysiol 96: 259–275, 2006.
First published March 29, 2006; doi:10.1152/jn.00687.2005.

Interhemispheric Integration at Different Spatial Scales: The Evidence From EEG Coherence and fMRI

Maria G. Knyazeva,[1,2,*] Eleonora Fornari,[1,*] Reto Meuli,[1] and Philippe Maeder[1]
[1]*Departments of Radiology and* [2]*Neurology, Centre Hospitalier Universitaire Vaudois, Lausanne, Switzerland*

Submitted 30 June 2005; accepted in final form 27 March 2006

Knyazeva, Maria G., Eleonora Fornari, Reto Meuli, and Philippe Maeder. Interhemispheric integration at different spatial scales: the evidence from EEG coherence and fMRI. *J Neurophysiol* 96: 259–275, 2006. First published March 29, 2006; doi:10.1152/jn.00687.2005. The early visual system processes different spatial frequencies (SFs) separately. To examine where in the brain the scale-specific information is integrated, we mapped the neural assemblies engaged in interhemispheric coupling with electroencephalographic (EEG) coherence and blood-oxygen-level dependent (BOLD) signal. During similar EEG and functional magnetic resonance imaging (fMRI) experiments, our subjects viewed centrally presented bilateral gratings of different SF (0.25–8.0 cpd), which either obeyed Gestalt grouping rules (iso-oriented, IG) or violated them (orthogonally oriented, OG). The IG stimuli (0.5–4.0 cpd) synchronized EEG at discrete beta frequencies (beta1, beta2) and increased BOLD (0.5 and 2.0 cpd tested) in ventral (around collateral sulcus) and dorsal (parieto-occipital fissure) regions compared with OG. At both SF, the beta1 coherence correlated with the ventral activations, whereas the beta2 coherence correlated with the dorsal ones. Thus distributed neural substrates mediated interhemispheric integration at single SF. The relative impact of the ventral versus dorsal networks was modulated by the SF of the stimulus.

INTRODUCTION

The retinal image is processed by the neurons of the primary visual cortex, which have spatially restricted receptive fields and are selectively responsive to spatial frequency (SF). Receptive fields tuned to similar SF tile the visual field in a patch-by-patch manner. Therefore each location in the visual field is seen by overlapping receptive fields tuned to a continuum of various SF (De Valois and De Valois 1990; Issa et al. 2000; Tootell et al. 1988). Because of this organization, the visual system behaves as a set of spatial filters (Campbell and Robson 1968; De Valois and De Valois 1990; Wilson and Wilkinson 1997, 2002). Hence the concept of the SF channel explains the performance of an assembly of spatially dispersed neurons with similarly tuned receptive fields. Due to the activity- and attention-dependent plastic properties of receptive fields on a millisecond scale (Bair 2005; Boyton 2005; Yao and Dan 2005), the SF channel represents not an invariant structural entity but rather a dynamic neural network.

The human visual system may be described as being composed of four to six SF channels with a bandwidth between one and two octaves (Georgeson 1980). The coarse and fine SF seem to engage differently in perception (Dakin and Bex 2001; Morrison and Schyns 2001). Several hypotheses have been proposed to explain the psychophysical results. They range from postulating independent additive low (LSF)- and high (HSF)-frequency channels to proposing interactive ones (Loftus and Harley 2004; Morrison and Schyns 2001) and imply that separate neural circuits along the visual processing stream can work on different spatial scales. However, the existence of within-scale integrating mechanisms is not reliably confirmed by physiological methods. For example, the extrastriate mechanisms for face recognition are shown to be either SF selective (Curby et al. 2003; Gauthier et al. 2005; Winston et al. 2003) or invariant across SF (Eger et al. 2004; Grill-Spector et al. 1999), depending on the experimental paradigm used.

Therefore the question remains as to how and where in the visual brain the information derived locally on multiple scales is integrated. As mentioned in the preceding text, one can view SF channels as dynamic neural assemblies. The mechanism by which distributed cortical assemblies coordinate their activity might be their synchronization (Bressler 1995; Fries 2005; Singer 1993). In that case, the distributed assemblies processing different or distant features of a visual stimulus must synchronize their activity to integrate the features of the stimulus into a coherent percept. Moreover, if the synchronization is a carrier of integration, it must reflect the relatedness of the stimulus parts. And, indeed, animal and human experiments showed that "good Gestalt," i.e., continuous, iso-oriented, coherently moving stimuli, induce higher synchronization than "bad Gestalt," i.e., discontinuous, cross-oriented, randomly moving ones (Bertrand and Tallon-Baudry 2000; Eckhorn 1994; Engel et al. 1991; Gray et al. 1992; Singer 1999; Tallon-Baudry 2003).

We studied the interhemispheric model of "integration through synchronization." This model is of particular interest because of the anatomical constraints that it provides. Within-hemispheric cortical circuits are limited to operating on the information from contralateral visual hemifields. The coordination between the hemispheres of the results of processing is implemented through the cortico-cortical callosal connections (Innocenti 1986; Munk et al. 1995). In line with our hypothesis, we have shown that in humans and animals collinear gratings presented simultaneously in both hemifields increase the interhemispheric synchronization of EEG signals in the beta-band compared with similarly presented orthogonal gratings (Carmeli et al. 2005; Kiper et al. 1999; Knyazeva et al. 1999).

Furthermore, we have found a link between the interhemispheric beta-band synchronization and fMRI BOLD response.

* M. Knyazeva and E. Fornari contributed equally to this work.

Address for reprint requests and other correspondence: M. G. Knyazeva, Dept. of Neurology, CHUV, 1011 Lausanne, Switzerland (E-mail: Maria.Knyazeva@chuv.ch).

The costs of publication of this article were defrayed in part by the payment of page charges. The article must therefore be hereby marked "*advertisement*" in accordance with 18 U.S.C. Section 1734 solely to indicate this fact.

Within the region around the collateral sulcus, which is known to implement the intermediate level of spatial integration (Wilkinson et al. 2000), the collinear gratings induced activation proportional to the interhemispheric EEG synchronization (Knyazeva et al. 2006). Thus integrating stimuli across the visual field is associated with coupling between interhemispheric beta-synchronization and fMRI activation. This coupling offers a way of mapping networks involved in integration and, in particular, in scale-related integration. In fact, such an approach reduces the task to mapping synchronized assemblies responding to the stimuli of limited SF contents.

We hypothesized that integration at different spatial scales is implemented by distributed activated networks that synchronize at various EEG frequencies. We tested this hypothesis with the interhemispheric integration paradigm applied to grating stimuli at various SF. We have found independent synchronization of at least two narrow beta bands at each single SF. In both hemispheres, in the low beta frequencies, the synchronization correlated with the ventral activations (collateral sulcus and fusiform gyrus), whereas in the higher beta frequencies, with the dorsal ones (parieto-occipital fissure and intraparietal sulcus). The relative activation of the ventral versus dorsal networks was modulated by the SF of the stimulus.

METHODS

The EEG and fMRI experiments reported here were performed on the same subjects. All the procedures conformed to the Declaration of Helsinki (1964) by the World Medical Association concerning human experimentation and were approved by the local ethics committee of Lausanne University.

Subjects

Thirteen adults [7 women; mean age: 35 ± (SD) 7.6 yr, range: 27–51 yr] without known neurological or psychiatric illness and with normal or corrected-to-normal vision participated in similar EEG and fMRI experiments. Three of the subjects were left-handed. All subjects gave written informed consent.

Stimuli

The choice of bilateral visual stimuli (Fig. 1) was based on the fact that the information originating from the two hemifields is channeled to separate hemispheres and the fusion of the visual field relies on the callosal connections between visual cortical areas. Therefore with the stimuli lateralized to the hemifields, we tested cortical mechanisms, which can be "seen" by both EEG and fMRI methods.

In the EEG experiment, subjects were presented with a set of sine-wave luminance gratings in the frequency range of 0.25–8.0 cycles/° (cpd) with 1-octave steps between the stimuli (0.25, 0.5, 1.0, 2.0, 4.0, and 8.0 cpd). The stimuli were bilaterally iso-oriented (at all mentioned SF) and orthogonally oriented (0.5, 2.0, 8.0 cpd) gratings centered on a fixation point. *Iso-oriented gratings* (IG) consisted of two identical patches of collinear, downward-drifting horizontal gratings on both sides of the fixation point. *Orthogonally oriented gratings* (OG) consisted of a patch of horizontal downward-drifting gratings on one side and a patch of vertical rightward-drifting gratings on the other side. All the gratings had the Michelson contrast of 70%; unilateral patches measured 13.5 × 24° (width × height). They drifted with a temporal frequency of 2 Hz. To compensate for retinal naso-temporal overlap and possible imperfect gaze fixation, all the stimuli were separated from the vertical meridian of the visual field by a narrow stripe of background equal to 1° on each side. A uniform gray screen of same space-averaged luminance as the stimuli (32

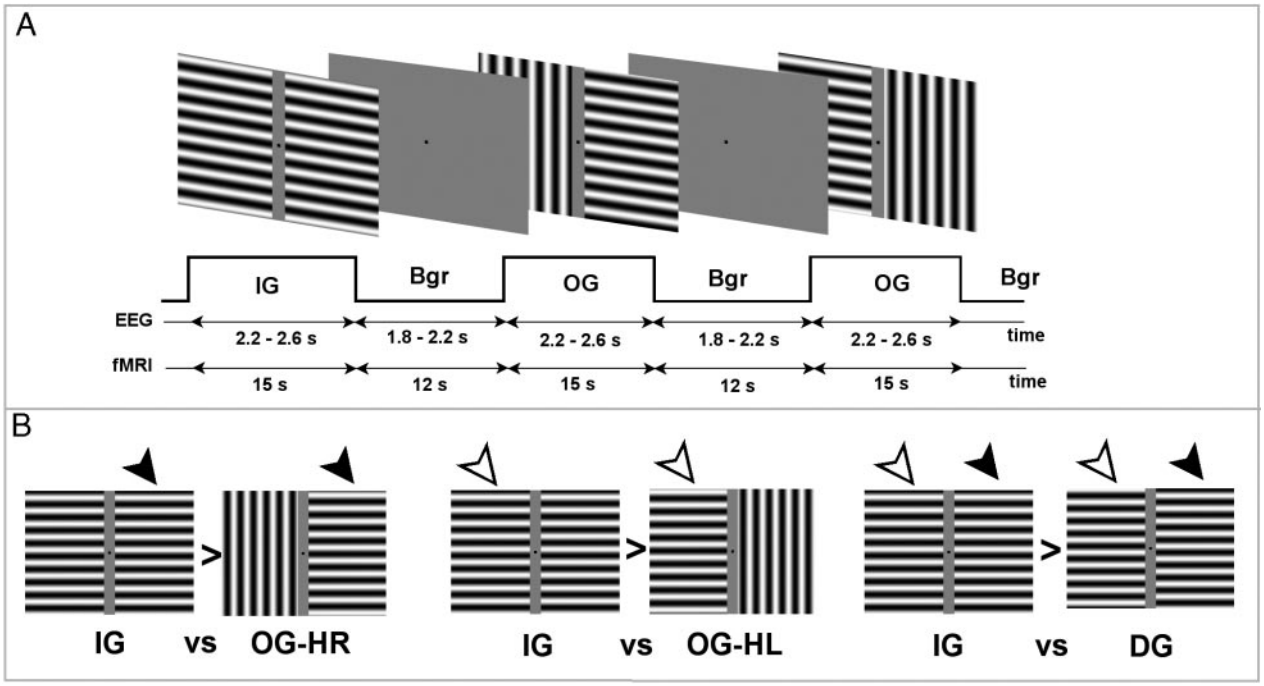

FIG. 1. The experimental paradigm for studying interhemispheric integration. *A*: examples of stimuli and the EEG fMRI protocols. In both EEG and fMRI sessions, subjects viewed bilateral iso-oriented (IG) or orthogonally oriented (OG) moving gratings projected on the two hemifields. In both experiments, we contrasted IG stimuli as facilitating integration between visual fields to perceptually segregated OG stimuli. In the EEG experiment, an increase in interhemispheric synchronization was targeted. In the fMRI experiment, we estimated *inter*hemispheric effects by contrasting activations induced by the same left or right horizontal grating (HL or HR shown by arrows of the same color) but under different conditions (IG vs. OG). These contrasts are shown in *B*. With additional dephased iso-oriented gratings (DG, on the *right*) applied only in the fMRI experiment (for details, see Knyazeva et al. 2006), we could expose the effect of interhemispheric interaction in both hemispheres simultaneously.

cd/m^2) with a fixation point in the center served as a *background* (Bgr).

During the EEG recording session, the stimuli were presented on a PC monitor with a refresh rate of 75 Hz. They were interleaved with the gray screen background. The vertical and horizontal gratings of the OG stimulus appeared in the left or right hemifield at random. Type of stimulus (OG, IG, and Bgr), stimulus exposure (2.2–2.6 s), and inter-stimulus intervals (1.8–2.2 s) were also randomized.

In the fMRI experiment, we presented a subset of gratings at 0.5 and 2 cpd to the same subjects. As our preliminary experiments had shown, stimuli at these SF induce maximum responses both in EEG coherence and in BOLD signal. Moreover, these gratings, separated by 2 octaves (the estimated width of a single spatial filter), are most likely processed by distinct spatial channels (Georgeson 1980). Due to technical problems, the 2 cpd data for two subjects were excluded from the respective analyses.

In the fMRI experiment, we tracked the effects of interhemispheric integration by evaluating responses of one hemisphere to the same horizontal gratings in the left or right visual field being coupled with one of the two co-stimuli in the opposite visual field (that is, with iso-oriented collinear gratings in IG condition, orthogonal gratings in OG condition). Consequently, contrasting IG > OG-HR (horizontal gratings in the right visual field) and IG > OG-HL (horizontal gratings in the left visual field), we assessed the effect of input variations in one hemisphere on the response to the nonchanging stimulus in another hemisphere.

Because the contrast IG > OG was not exhausted by interhemispheric effects but also included intrahemispheric ones due to the different gratings' orientation (Knyazeva et al. 2006), we applied a control stimulus, *dephased iso-oriented gratings* (DG). The DG was identical to IG except that the right and left sides of this stimulus were 180° out of phase. In IG > DG contrast the interhemispheric effect could be traced in both hemispheres simultaneously.

The stimuli alternated with a background in a balanced-randomized order. Each stimulus was displayed with an LCD projector five times for 15 s at a refresh rate of 75 Hz. The projector was equipped with a photographical zoom lens that projected images onto a translucent screen in a custom-made mirror box positioned inside the magnet. The mirror box was designed to minimize light reflections. It allowed a subject to view the stimuli within the space defined by 25° horizontally and by 19° vertically.

Because EEG/LFP synchronization in response to moving gratings sustains for periods much longer than used in our EEG recordings (Eckhorn 1994; Kiper et al. 1999; Munk and Neuenschwander 2000), our experimental design preserved compatibility of the EEG and fMRI results in spite of the different time scales. In both experiments, subjects were asked to maintain fixation while viewing stimuli. Subjects were also instructed to refrain from blinking during stimulus presentation. Their fixation was monitored by the experimenter during the EEG (all subjects), and with an eye tracking system during the fMRI recording session (5 subjects). The eye-tracking data, on-line EEG monitoring, and off-line EEG analysis confirmed that subjects followed these instructions most of the time (see the following sections for details).

Control of eye movements

To remove EEG epochs contaminated with eye blinks and/or eye movements, we used artifact detection tools implemented in the NS3 software (Electrical Geodesics, Eugene, OR). These algorithms are based on differential thresholds applied to the three pairs of eye channels, which we specified as 70 μV. Thus if the difference between fast and slow running averages of vertical eye channel deviation or horizontal eye-channel deviation exceeded 70 μV, the tool marked the segment as bad.

During the fMRI session, we monitored five subjects with an eye tracking system (SensoMotoric Instruments GmbH, Teltow, Germany). For the calibration of subjects' point of gaze, we used the built-in 9-point routine. Time locking between eye-movement data and experimental condition was achieved via triggering the eye-tracking system by an in-house made program for stimulus presentation. Eye positions were sampled at 50 Hz and stored on a PC for off-line analysis with Matlab. The readings for 0.25 s before and 0.5 s after the start of a blink, when gaze position cannot be determined, were removed from analysis (<2.5% of the acquisition time). We assessed fixation stability as a percentage of time when the point-of-gaze was within a circle (Ø 2°) centered on a fixation point—that is, within the gap in bilateral stimuli. All the subjects showed permanent fixation for 96–99% of the recording time across all the conditions (the results are published in Knyazeva et al. 2006).

EEG recording and processing

The EEG data were collected in a semi-dark room with a low level of environmental noise. The subject was sitting in a comfortable chair. The subject was instructed to fixate on the point in the center of the screen located at a distance of 57 cm. To stabilize the head position and maintain this distance, we used an adjustable chin-rest mounted on a table in front of the subject. The EEGs were recorded with the 128-channel Geodesic Sensor Net (Tucker 1993). In RESULTS, the sensor numbers are supplemented where possible with designations according to the international 10–20 system. All the electrode impedances were kept <50 kΩ as recommended for the high-input-impedance EGI amplifiers (Ferree 2000; Picton et al. 2001). The on-going EEG tracings were constantly monitored during the experiment to keep the quality of recording and the subject's wakefulness level under steady watch.

The recordings were made with vertex reference using a low-pass filter set to 100 Hz. The signals were digitized at a rate of 500 samples/s with a 12-bit A/D converter. They were further filtered (FIR, band-pass of 3–70 Hz,[1] notch of 50 Hz), re-referenced against the common average reference, and segmented into nonoverlapping epochs using NS3 (Electrical Geodesics) software. The choice of the common average reference for the EEG coherence measurements with dense array EEG is discussed elsewhere (Knyazeva et al. 2006). Artifacts in all channels were edited off-line: first, automatically, based on an absolute voltage threshold (100 μV) and on a transition threshold (50 μV) and then through thorough visual inspection, which allowed us to identify and to reject epochs or channels with moderate muscle artifacts not reaching threshold values. On average 16% of epochs were excluded from further analysis.

Estimates of coherence depend on the choice of EEG reference (Nunez et al. 1997, 1999). In our previous studies, we have shown that interhemispheric coherence dynamics under experimental conditions similar to the ones applied here is replicable across different reference techniques and that the common average reference (AR) is the most appropriate choice (Knyazeva et al. 1999, 2006).

To minimize the impact of stimulus-onset artifacts and response-onset transients together with stimulus-locked synchronization, we excluded the first 200–220 ms (randomized across subjects) after stimulus onset (for detailed discussion, see Knyazeva et al. 2006). FFT was applied to 1-s EEG segments (1-Hz frequency resolution). For each individual, ≥45 artifact-free epochs were collapsed for each stimulation condition to obtain coherence and power spectra. EEGs with <110 good channels were excluded from further analysis. The spectral analysis was centered on EEG coherence functions as an index of functional interactions between brain regions.

[1] The choice of filtering options was justified by the focus of this research on the beta band. It was not optimal for low-frequency EEG and, therefore, could have affected the results obtained in the theta band.

EEG spectral analysis and statistics

For spectral analysis, MATLAB routines were used (Srinivasan et al. 1998). For the analysis of stimulus-induced changes we used *magnitude-squared-coherence* (MSC)**.** At a frequency f, it is defined by the formula

$$\mathrm{Coh}(f) = |S_{xy}(f)|^2/(S_{xx}(f)*S_{yy}(f))$$

where S_{xx}, $S_{yy,}$ and S_{xy} are auto- and cross-spectrum estimates of the x and y signals. Scalp surface coherence maps were created by spherical interpolation and plotted in polar projection (Perrin et al. 1989). Further analysis was focused on interhemispheric coherence (ICoh) between EEG signals recorded from symmetrically placed electrodes. To stabilize the variance, we applied an arc hyperbolic tangent transformation to the measured ICoh (Halliday et al. 1995).

The $\tanh^{-1}$ coherences were subjected to the Student's t-test for paired samples. We performed this test at each single frequency across the 4- to 47-Hz range. Because we used the Student's t-test as an exploratory tool to identify the region of interest (i.e., sensor pairs of interest) and the EEG frequency range of interest for further analysis, no correction for multiple comparisons was applied.

The EEG band selected by preliminary analysis as containing systematic ICoh changes associated with stimulation was further subjected to principal component analysis (PCA). The purpose of PCA was to study the structure of the responsive frequency range and to reduce the number of variables for further analysis (Arruda et al. 1996). Prior to PCA, the suitability of the data sample for factor analysis was tested with the Kaiser-Meyer-Olkin (KMO) measure of sampling adequacy and with Bartlett's test of sphericity (Kaiser 1974). The KMO was 0.762, exceeding the recommended value of 0.6, and Bartlett's test of sphericity (Pallant 2001) was highly significant ($P < 0.001$), showing good factorability of the data. PCA was performed on a correlation matrix. We have chosen to use an orthogonal varimax rotation based on the observation that in our empirical data ICoh responses at low and high beta frequencies are uncorrelated. To extract principal components, we used Kaiser's eigenvalue representing the amount of the total variance explained by a given factor. Components with eigenvalue >1 were extracted. To reach a reliable solution, we considered only components composed of three or more variables strongly correlated with the factor that is composed of variables with loadings >0.6 (Velicer and Fava 1987). Variables highly correlated with independent components were subjected to a repeated-measures ANOVA to assess the effects of SF, electrode location, and ICoh response frequency. All the statistical tests we used were implemented in SPSS 10.0 for Macintosh (SPSS).

fMRI protocol and preprocessing

BOLD fMRI acquisitions were performed with a head coil on a 1.5 Tesla Siemens (Erlangen, Germany) Magnetom Vision system equipped for echoplanar imaging. The subject's head was cushioned in the coil with a vacuum beanbag to prevent motion. fMRI images were acquired with an EPI gradient echo T2*-weighted sequence (FA 90, TE 66, pixel size: 3.75 * 3.75 mm, acquisition time: 1.7 s, 16 slices of 5 mm with a gap of 1 mm) with a TR = 3 s for a total of 25 acquisitions for each stimulus. fMRI preprocessing steps, conducted with SPM2 (Wellcome Department of Cognitive Neurology, London, UK), included realignment of intra-session acquisitions to correct for head movement, normalization to a standard template [Montreal Neurological Institute (MNI) template] to minimize inter-subject morphological variability, and convolution with an isotropic Gaussian kernel [full-width half-maximum (FWHM) = 9 mm] to increase signal-to-noise ratio. Single-subject analysis was performed according to the general linear model. The signal drift across acquisitions was removed with a high-pass filter (the cut-off frequency being 0.005 Hz), and global signal changes by proportional scaling. Statistical parametrical maps of the contrasts ofinterest were computed for each subject as input values for the group statistics based on random field theory. In particular, the inferential statistics included a repeated-measures ANOVA and t-test. Only clusters with the height threshold set at $P < 0.01$ and the extended threshold $k > 30$ contiguous voxels corresponding to $P < 0.05$ (corrected) were considered significant in all the contrasts of interest unless stated otherwise.

Anatomical identification and the display of results

A sagittal T1-weighted three-dimensional (3D) gradient-echo sequence (MPRAGE), 128 slices (with voxel size of 1*1*1.25 mm), was acquired as the structural basis for brain segmentation and surface reconstruction.

High-resolution morphological acquisitions were segmented, inflated, and flattened by Freesurfer software (http://surfer.nmr.mgh.harvard.edu) following standard procedures (Dale et al. 1999; Fischl et al. 1999). In addition to the standard SPM display, group data were exported, denormalized, and displayed on a single subject's cortical flattened surface. We identified the anatomical location of cluster boundaries and centers via transformation of MNI coordinates into Talairach space (McKeefry and Zeki 1997; McKeefry et al. 1997; Zeki 1993). Cluster positions were verified according to individual anatomical landmarks.

To check the EEG electrodes' positions against brain morphology and fMRI BOLD responses, in five subjects, adhesive radiographic markers (MM3002, IZI Medical Product, Baltimore, MD) were attached to the skin in the locations of occipital and parietal Geodesic Net sensors as well as in standard skull landmarks including nasion, inion, preauricular notches, and vertex; these radiographic markers were co-registered with fMRI followed by 3D reconstruction of MRI morphological images of the head.

EEG coherence—fMRI BOLD correlation analysis

Correlation analysis estimates linear relationships between measured parameters. To make it more reliable, we adjusted our experimental design to minimize known nonlinearities in the hemodynamic and neuronal responses (Bandettini and Ungerleider 2001; Boynton et al. 1996; Friston et al. 2000). To this end, we applied drifting gratings as stimuli because they induce sustained EEG synchronization (Munk and Neuenschwander 2000) and hemodynamic response (Kayser et al. 2004; Niessing et al. 2005) on a second scale. In the EEG experiments, we avoided on and off effects as well as the effects of habituation and fatigue on repeated trials by limiting the duration of experiments and randomizing trials. In the fMRI experiments, we used a block design with block length of 15 s and with inter-stimulus intervals of 12 s sufficient to avoid interaction between adjacent responses (Boynton et al. 1996).

The region of interest (ROI) for the correlation analysis was selected as all the voxels activated with any one of the stimuli used. To test the relationship between distant synchronization and BOLD, we have chosen IG > OG contrast because, in this contrast, the ICoh increase was not confounded with the EEG power changes (see RESULTS). As a predictor variable we used $\sqrt{}$MSC (see *EEG spectral analysis and statistics*), which is analogous to the bivariate correlation coefficient and measures linear association between two EEG signals in a frequency domain. For each subject, we derived difference scores by subtracting OG-$\sqrt{}$MSC values from IG-$\sqrt{}$MSC values at each frequency of interest. The individual BOLD changes from the IG > OG contrast served as an outcome (dependent) variable. In particular, percent signal change for each voxel within the ROI went into the computation. Thus correlations were performed on a voxel-by-voxel basis. We calculated the distributions of correlation coefficients between $\sqrt{}$MSC and BOLD, and thresholded the results for peak height

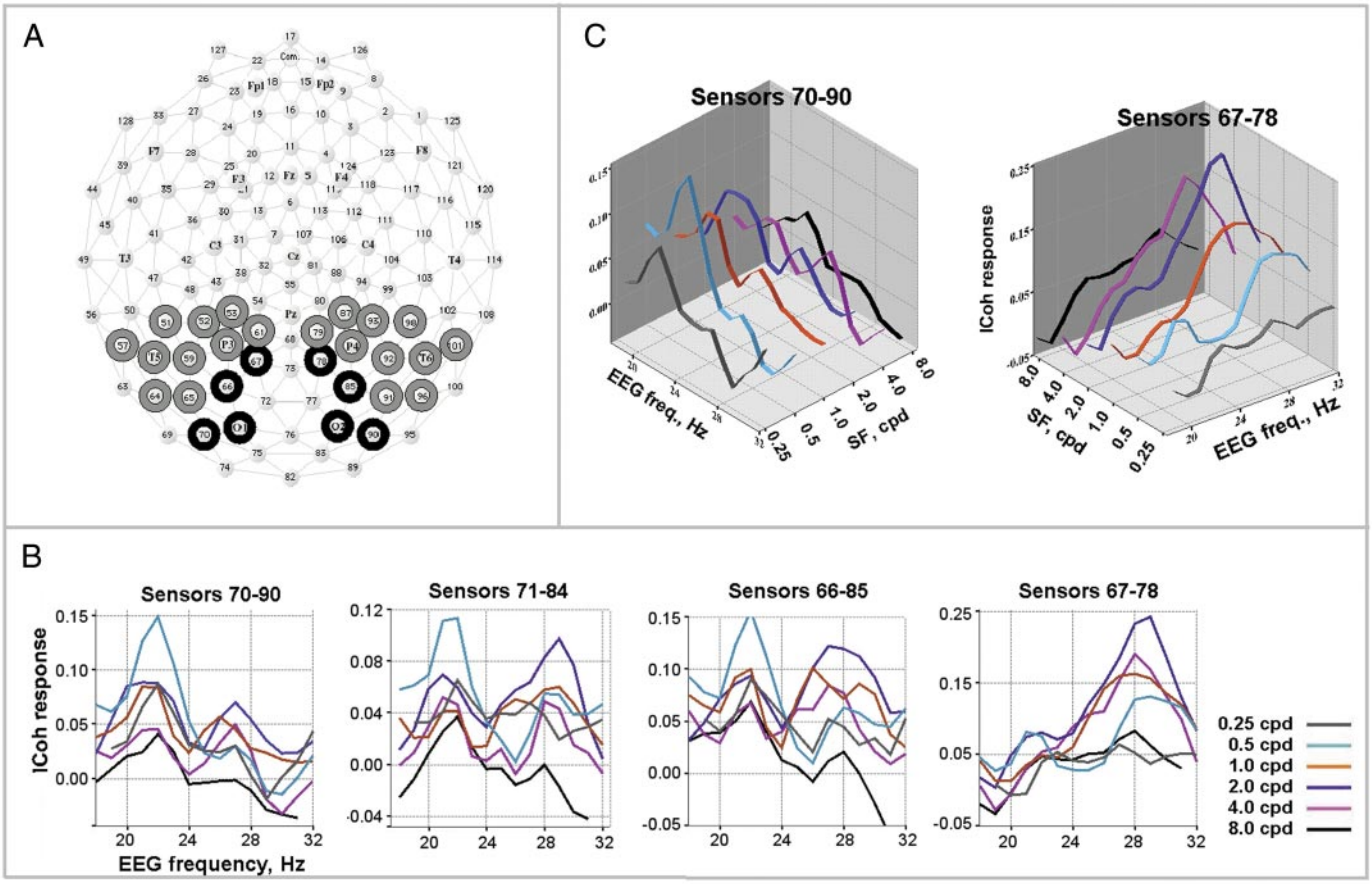

FIG. 2. Interhemispheric EEG tauh-1 coherence under stimulation by collinear gratings over a range of spatial frequencies. In *A,* schema of 128-channel Geodesic Sensor Net with sensors screened for interhemispheric coherence (Icoh) responses to IG stimulus in gray and with statistically confirmed responses in black. In *B,* the group-averaged ICoh responses are shown as difference spectra (IG > Bgr) in the spatial frequency (SF) range between 0.25 and 8.0 cpd. In *C,* the ICoh responses from sensors pairs with dominant peaks at 22 Hz (sensor pair 70–90) and 28 Hz (sensor pair 67–78) are visualized in 3-dimensional (3D) rendered images.

at $P < 0.01$ and for spatial extent at $k \geq 20$ contiguous voxels (i.e., at k larger than the minimum number of voxels expected per cluster) (Friston et al. 1993). The generated correlation maps show only clusters reaching a significance level of P (corrected) < 0.05.

RESULTS

EEG synchronization

We have reported elsewhere that IG increases ICoh compared with Bgr or OG. The effects we reported were specific for the beta-band and for derivations located over the occipito-parietal cortex [based on the conventional (Knyazeva et al. 1999) and on the high-density (Carmeli et al. 2005; Knyazeva et al. 2006) EEG]. These reports describe EEG synchronization effects in response to sine gratings with an SF of 0.5 cpd. Here we examine whether the ICoh response depends on the spatial frequency of grating stimuli in the range of 0.25–8.0 cpd.

SEARCHING FOR ROI AND RESPONSIVE EEG BAND. An ROI was defined in a preliminary exploratory analysis of the group data. The analysis was based on a Student's paired *t*-test. It was applied to each EEG frequency between 4 and 47 Hz obtained from each of 14 symmetrically placed interhemispheric sensor pairs at posterior locations (Fig. 2A). We contrasted each of six iso-oriented gratings at SF 0.25–8.0 cpd against the background. The ICoh responses at $P < 0.05$ (uncorrected) were selected for further analysis.

The test showed that only the ICoh responses in the range of 0.5–4.0 cpd (Fig. 2, *B* and *C*) met this significance criterion. The lowest (0.25 cpd) and highest (8.0 cpd) SF failed to induce ICoh increase even with this liberal statistical approach. The responsive sensors 70–90, 71–84, 66–85, and 67–78 (128-channel Geodesic Net), located over the occipital and parietal cortices, were spaced 6–9 cm apart. The ICoh increased within the beta-gamma range (20–31 Hz).[2] In particular, the stimuli induced ICoh responses at 21–23 Hz at occipital and at 26–28 Hz at parietal locations. The low-frequency beta peak predominated at low SF, while the higher-frequency beta peak prevailed at higher SF; the effects could be seen even in individual subjects' data (Figs. 3 and 4).

Spatial selectivity of these effects is represented in Fig. 4 by means of difference maps of coherence. As is clear from this picture, in spite of inter-individual variability, under IG stimulation the EEG signals recorded over the left occipital and parietal cortices are synchronized with the EEG signals re-

[2] The exploratory analysis excluded EEG spectral power density in the frequency range of interest from further consideration, for it carried no systematic changes across stimulation conditions (IG > Bgr and IG > OG). For details see also Knyazeva et al. (2006).

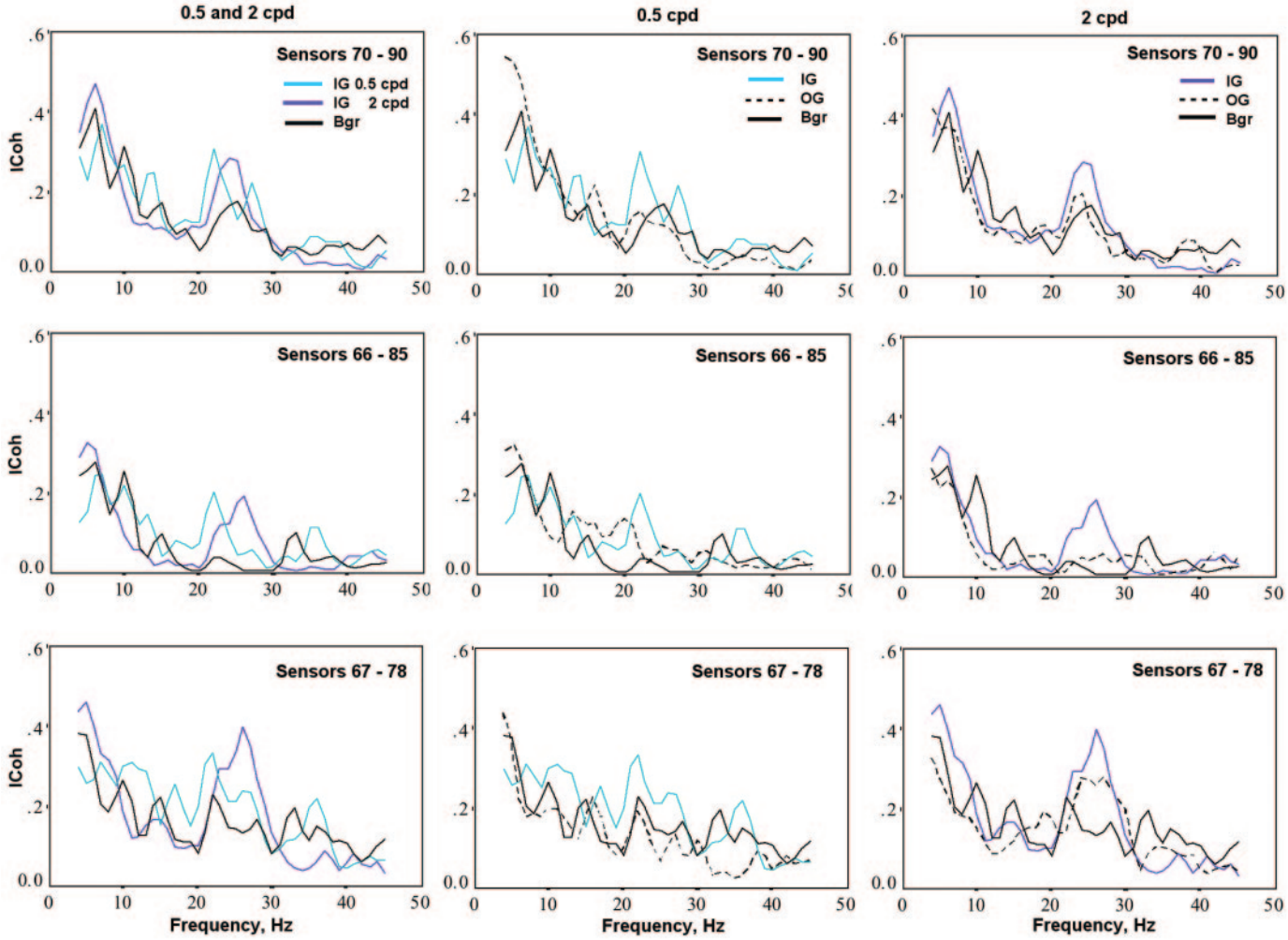

FIG. 3. The individual ICoh spectra from a representative subject (YY) computed for common average reference EEG from the occipital and parietal sensor pairs 70–90, 66–85, and 67–78 are shown. These sensor pairs represent the lowest, 1 intermediate, and the highest locations marked in black in Fig. 2*A*.

corded over occipital and parietal areas of the right hemisphere (marked with red) at beta1 and beta2 EEG frequencies. Notably, these EEG signals do not synchronize with the signals from close occipital, parietal, and temporal locations that are ipsilateral to the referent sensors 70 and 67 (green or blue). The selectivity of EEG coherence responses both in temporal and in spatial domains points toward their true interhemispheric sources.

The peak response frequencies seemed to be stable across EEG sensors and SF and suggested a certain structure of the beta band presumably characterized by independent responses at low and high frequencies within the 20- to 31-Hz range.

TESTING THE STRUCTURE OF THE RESPONSIVE EEG BAND. To test the structure of the beta band, we subjected to PCA the ICoh estimates for individual subjects at all the frequencies in the 20- to 31-Hz range across the four sensor pairs and at all IG conditions (78 cases in total). The analysis resulted in orthogonal components, which represented either the whole frequency band at parietal or occipital sensor locations (principal components 1–2, explaining 45.6% of variance), or sub-bands (principal components 3–6, explaining 26.1% of variance). The latter components included rather narrow frequency ranges either across several sensor pairs or restricted to a single sensor pair (Fig. 5A). More precisely, they included one low (21–23 Hz) and two high-frequency ranges (26–28 and 29–31 Hz), which will be referred to as beta1, beta2, and beta3 components, respectively. The application of PCA to individual IG conditions in the 0.5- to 4.0-cpd range showed the reproducibility of the main features of the beta-band structure. The principal components that emerged at 0.5 and 2.0 cpd are particularly noteworthy because these SF were used for further ICoh/fMRI analysis. As can be seen from Fig. 5, *B–D*, each principal component incorporated similar beta frequencies across stimuli. Furthermore, these beta-components corresponded to the responsive EEG frequencies. In particular, the 22- and 28-Hz peaks had high loadings (up to >0.9) on the beta1 and beta2 components, respectively. Overall, the PCA results indicated that high and low EEG beta frequencies are involved in relatively independent processes of interhemispheric synchronization induced by visual stimulation.

ANOVA: THE EFFECTS OF SPATIAL FREQUENCY, LOCATION, AND EEG FREQUENCY. We performed a repeated-measures ANOVA with the SF (3 levels), sensor location (4 levels), and EEG response peak (3 levels) factors. The choice of the SF levels was dictated by the following considerations. In humans, a spatial channel width is <2 octaves (De Valois and De Valois

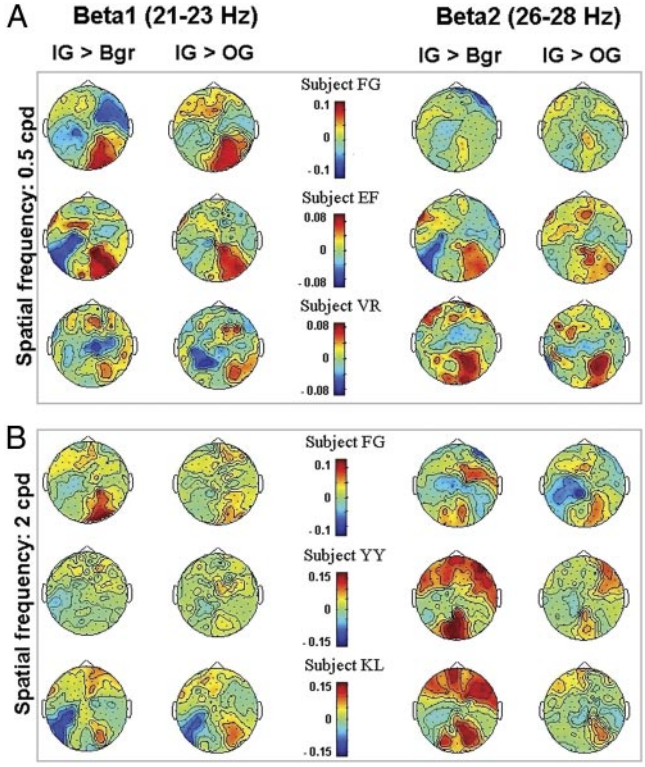

FIG. 4. Difference maps of the EEG coherence from individual subjects (rows) for the IG > Bgr and IG > OG contrasts (columns). *Left*: coherence changes for the beta1 factor; *right*: coherence changes for the beta2 factor. The beta1 maps are plotted with respect to sensor 70, the beta2 maps with respect to sensor 67 (see the scheme of 128-channel Geodesic Sensor Net in Fig. 2*A*). The responses to stimulation by gratings at 0.5 cpd are shown on *A,* with 2 cpd on *B.*

1990). Therefore by contrasting 0.5 versus 2 and versus 4 cpd, we compared distinct channels. The sensor location factor contrasted occipital and parietal sensor pairs. The EEG response peak factor distinguished ICoh responses at peak frequencies of 22, 28, and 31 Hz. As a dependent variable, we used the $\tanh^{-1}$-transformed ICoh responses (IG vs. Bgr) averaged in individual subjects' data for each stimulus condition and sensor pair.

There was a highly significant main effect for the sensor location factor [$F(3,36) = 7.64$, $P < 0.001$ (the sphericity assumption, assessed using Mauchly's test of sphericity, has been met)]. The sensor location factor also significantly interacted with the EEG peak response factor [$F(4.7,56.57) = 3.57$, $P = 0.008$ with Huynh-Feldt correction]. This interaction suggests that, averaging across SF, the ICoh responses at different beta-frequencies differ for the sensor pairs under analysis. Indeed, planned comparisons confirmed that the ICoh increase was higher at the parietal than at the occipital location (sensor pair 67–78 vs. 70–90) for the peaks at 28 and 31 Hz ($P < 0.05$, corrected). Within this range of SF, the main effect of SF and its interactions was not significant, which could have been expected because of the nonlinear relationship between SF and ICoh response (Fig. 2, *B* and *C*).

EFFECTS OF STIMULUS: ISO-ORIENTED VERSUS ORTHOGONALLY ORIENTED GRATINGS. To isolate the effects of interhemispheric interaction, we contrasted ICoh responses to IG versus OG stimuli at 0.5 and 2.0 cpd (Figs. 3 and 4). These SF were chosen because they induced robust responses both in EEG and in fMRI sessions. The repeated-measures ANOVA with stimulus (2 levels: IG, OG), spatial frequency (2 levels: 0.5 vs. 2.0 cpd), and sensor location (4 levels, as in the preceding text) factors confirmed greater ICoh increase under the IG compared with the OG condition at peak response frequencies 22 and 28 Hz [$F(1,12) = 4.31$, $P = 0.06$ and $F(1,12) = 7.60$, $P = 0.017$, respectively; the sphericity assumption has been met]. The interaction between stimulus and spatial frequency indicative of the dominance of the low beta at 0.5 cpd and of the high beta response at 2.0 cpd was significant for 22 Hz ($P = 0.05$) and marginally significant for 28 Hz ($P < 0.1$).

In brief, we have found that for the gratings at SF 0.5–4.0 cpd, the EEG beta range between 20 and 31 Hz contained narrow subbands responsive to stimulation with iso-oriented bilateral gratings. The ICoh measures at these frequencies showed noncorrelated behavior and differentiated the good-Gestalt from the bad-Gestalt stimuli. Therefore the ICoh response peaks could signify synchronization in distributed neural populations. The fMRI experiments have been designed to test this hypothesis.

BOLD response

Because preliminary trials had shown that the intensity of the BOLD response to the stimuli decreases with increasing SF, we limited the fMRI experiments to the low (0.5 cpd, LSF) and medium (2.0 cpd, MSF) SF gratings. A two-way repeated-measures ANOVA was applied to reveal the effects of SF and

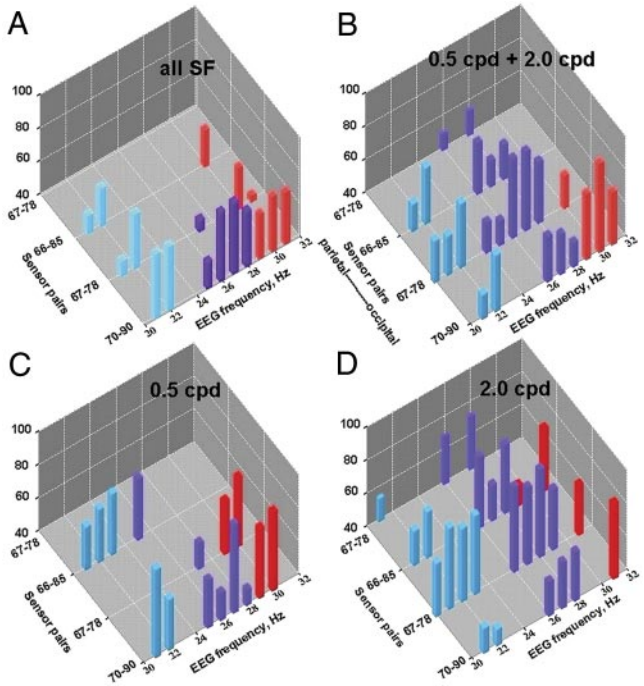

FIG. 5. Loadings of the original coherence variables on the beta-factors. The 3D graphs represent ICoh loadings on selected principal components. One horizontal axis shows EEG spectral frequency (20–32 Hz), the other – sensor pairs. The scaled vertical bars stand for loadings of ≥0.5. Factors represent beta subbands and are distinguished using color. Low beta factor (blue) includes ICoh at 21–23 Hz. High beta factor (violet) receives higher loadings exclusively from 26 to 28 Hz. Another high beta factor (red) describes ICoh in the 29- to 31-Hz band. Note the consistency of factor patterns across spatial frequencies (*C* and *D*) and their combinations (*A* and *B*).

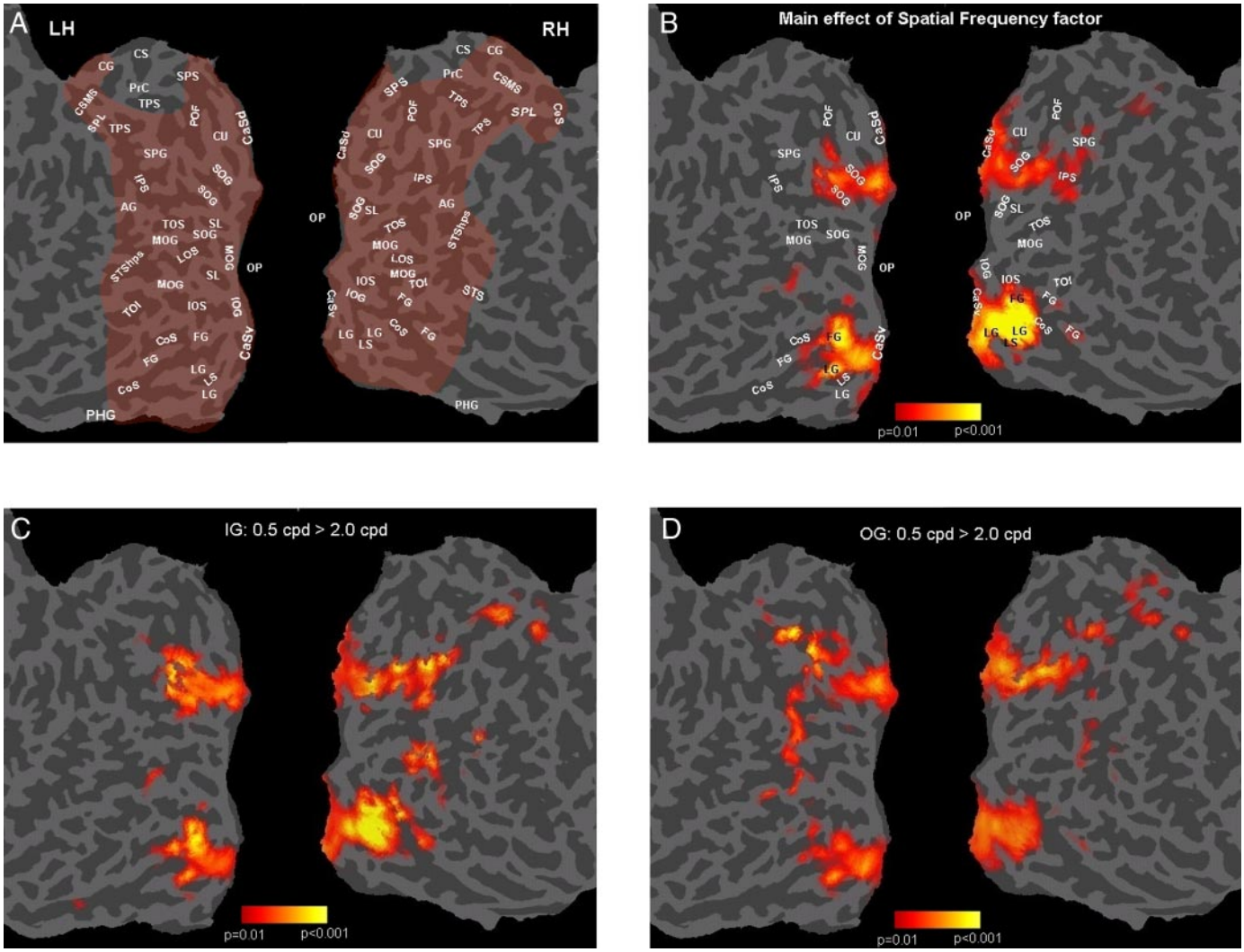

FIG. 6. Functional activation maps for the group data showing the effects of spatial frequency on the BOLD response. The functional activations, denormalized according to individual inverse transformation, are superimposed on flattened cortical surfaces of the right and left hemispheres (LH and RH, respectively) of a single subject's brain. The sulci are coded in darker gray than the gyri. A: detailed anatomy of the region of interest (ROI) is presented. The ROI, shown in transparent color, was defined as the set of all the voxels activated in ≥1 of the contrasts. The ANOVA main effect of the spatial frequency factor is in *B*. The 2 contrasts supporting it (0.5 cpd > 2 cpd for IG and OG stimuli at $P < 0.01$) are shown in *C* and *D,* respectively. AG, angular gyrus; CaSd, calcarine sulcus (dorsal part); CaSv, calcarine sulcus (ventral part), CoS, collateral sulcus; CS, cingulate sulcus; CSMS, cingulate sulcus (marginal segment); CU, cuneus; FG, fusiform gyrus; IOG, inferior occipital gyrus; IOS, inferior occipital sulcus; IPS, intra-parietal sulcus; ITG, inferior temporal gyrus; ITS, inferior temporal sulcus; LG, lingual gyrus; LOS, lateral occipital sulcus; LS, lingual sulcus; MOG, middle occipital gyrus; MTG, middle temporal gyrus; PHG, parahippocampal gyrus; POF, parieto-occipital fissure; PrC, precuneus; SL, sulcus lunatus; SOG, superior occipital gyrus; SPG, superior parietal gyrus; SPL, superior parietal lobule; STShps, superior temporal sulcus (horizontal posterior segment).

stimulus on the BOLD response. The effects were mapped separately in Figs. 6 and 7 on an individual flattened brain.

ANOVA: THE EFFECTS OF SPATIAL FREQUENCY AND STIMULUS. The main effect of the SF factor ($P < 0.001$) showed that the LSF gratings activated the visual areas more strongly than the MSF gratings, regardless of the stimulus category (Fig. 6). Significantly different activations were located bilaterally on both banks of the calcarine sulcus (V1, V2) in their middle and anterior parts, but spared the occipital pole (Fig. 6*B*). Ventrally, it extended to the lingual gyrus (VP), dorsally, to the cuneus (V3d), and, along the inferior bank of the parieto-occipital fissure, it reached the superior occipital gyrus. In the right hemisphere, the impact of the SF factor was stronger and extended further anteriorly, through the first parieto-occipital bridging lobule to the superior parietal gyrus and the intraparietal sulcus (IPS). The contrasts 0.5 > 2.0 cpd performed for each stimulus type separately (IG, OG, and DG) supported the SF main effect (Fig. 6, *C* and *D*). The opposite contrasts (2.0 > 0.5 cpd) did not show any clusters that were activated more strongly with the MSF stimuli.

The analysis of the stimulus factor revealed changes in the extrastriate activations ($P < 0.01$) induced by IG versus OG, regardless of SF (Fig. 7*A*). They were located bilaterally in the fusiform gyrus and inferior occipital sulcus (V4). We analyzed only contrasts that exposed the effects of interhemispheric integration (good-Gestalt > bad-Gestalt). These were the IG > OG-HR, IG > OG-HL, and IG > DG contrasts at each SF. Across the contrasted conditions, one hemisphere "saw" the

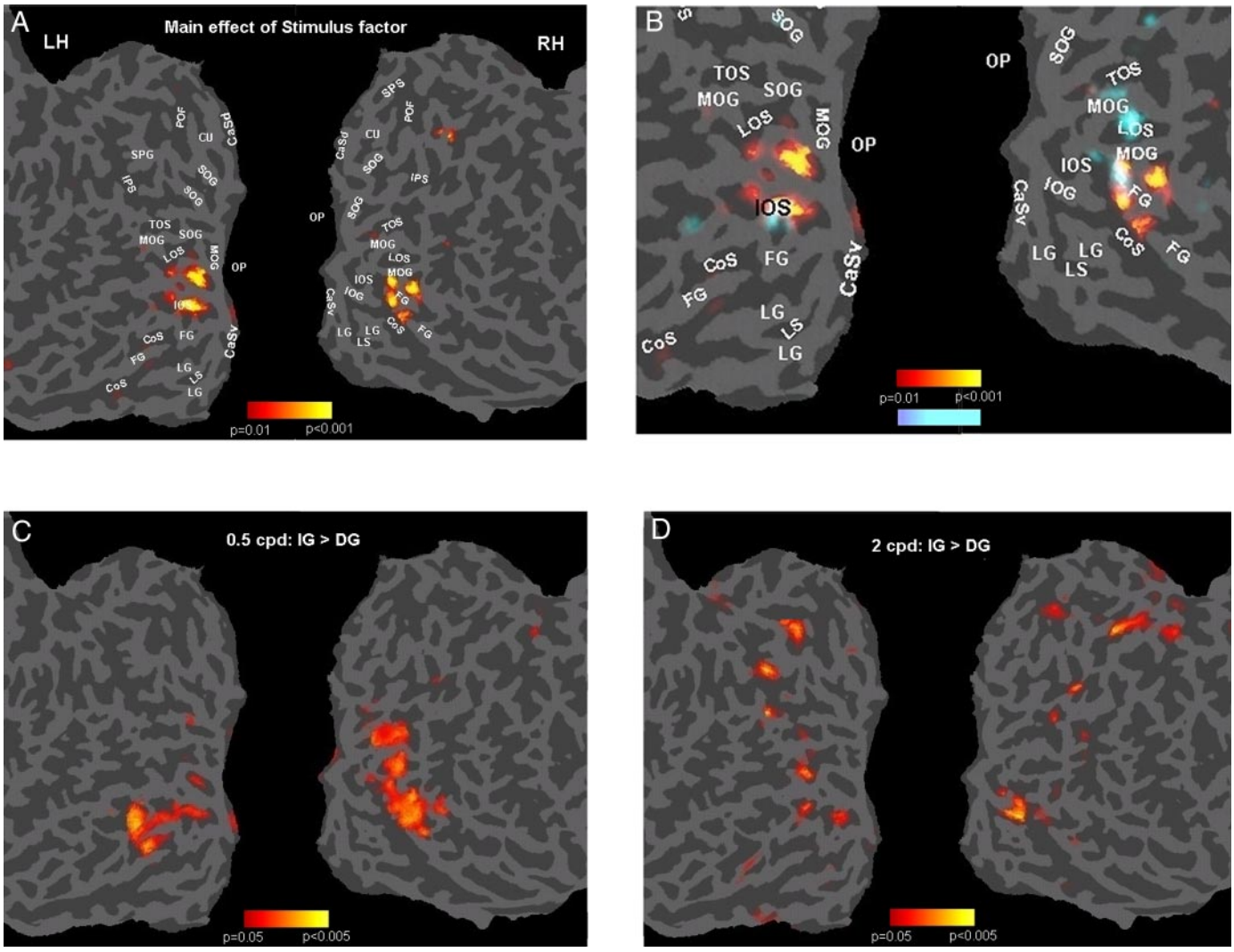

FIG. 7. Functional activation maps for the group data showing the interhemispheric integration effects. *A*: main effect of the stimulus factor ($P < 0.01$) is superimposed on a single subject's parieto-occipital flat map. An enlarged view of the ventral location with the interaction between SF and stimulus (light blue, $P < 0.01$) superposed on the main effect of stimulus is depicted in *B*. The 2 contrasts in *C* and *D* (IG > DG at 0.5 and at 2.0 cpd, respectively) exemplify both the stimulus effect and its interaction with SF. Other designations are as in Fig. 6.

same horizontal gratings, whereas input to the other hemisphere varied. Thus variations in the response to the horizontal grating "seen" by one hemisphere could be ascribed to interactions with the stimulus "seen" by the other hemisphere.

We found higher activations in response to the horizontal stimulus under the IG condition (i.e., with a collinear grating being presented to the other hemisphere) compared with both the OG and DG conditions (i.e., when the other hemisphere "saw" orthogonal or out-of-phase gratings). The difference was significant in five of six contrasts including all the contrasts for 0.5 cpd and the IG > DG and IG > OG-HR contrasts for 2.0 cpd. The IG > OG-HL contrast, which was intended to show the interhemispheric effect in the right hemisphere, did not reach statistical significance, though the IG > DG contrast clearly revealed an interhemispheric effect in both hemispheres (Fig. 7, *C* and *D*).

INTERACTION BETWEEN THE MAIN EFFECTS OF SPATIAL FREQUENCY AND STIMULUS. The interaction between the stimulus and spatial frequency factors was expected to map activations involved in the interhemispheric integration specifically at LSF or MSF. It was found to be significant at $P < 0.05$ for certain ventral and dorsal locations (Fig. 7*B*). The ventral clusters were located bilaterally along the posterior part of the collateral sulcus and along the inferior occipital sulcus, and in the right lateral occipital sulcus. In these ventral locations, the stimulus effect (IG > OG, IG > DG) was stronger at the LSF than at the MSF predominantly in the right hemisphere (Fig. 7, *C* vs. *D*). Dorsal clusters have been found bilaterally in the parieto-occipital fissure (POF), IPS, and in the transverse parietal sulcus. In these dorsal locations, the responses (IG > DG, IG > OG-HR) were significant ($P < 0.01$) at 2.0 cpd but not at 0.5 cpd. They were more salient in the left hemisphere.

Therefore BOLD dynamics revealed areas associated with interhemispheric integration whose activation does not vary across SF (ventral extrastriate locations) and areas where activation is modulated by SF (ventral and dorsal locations). Among the regions tuned to SF, ventral locations showed a

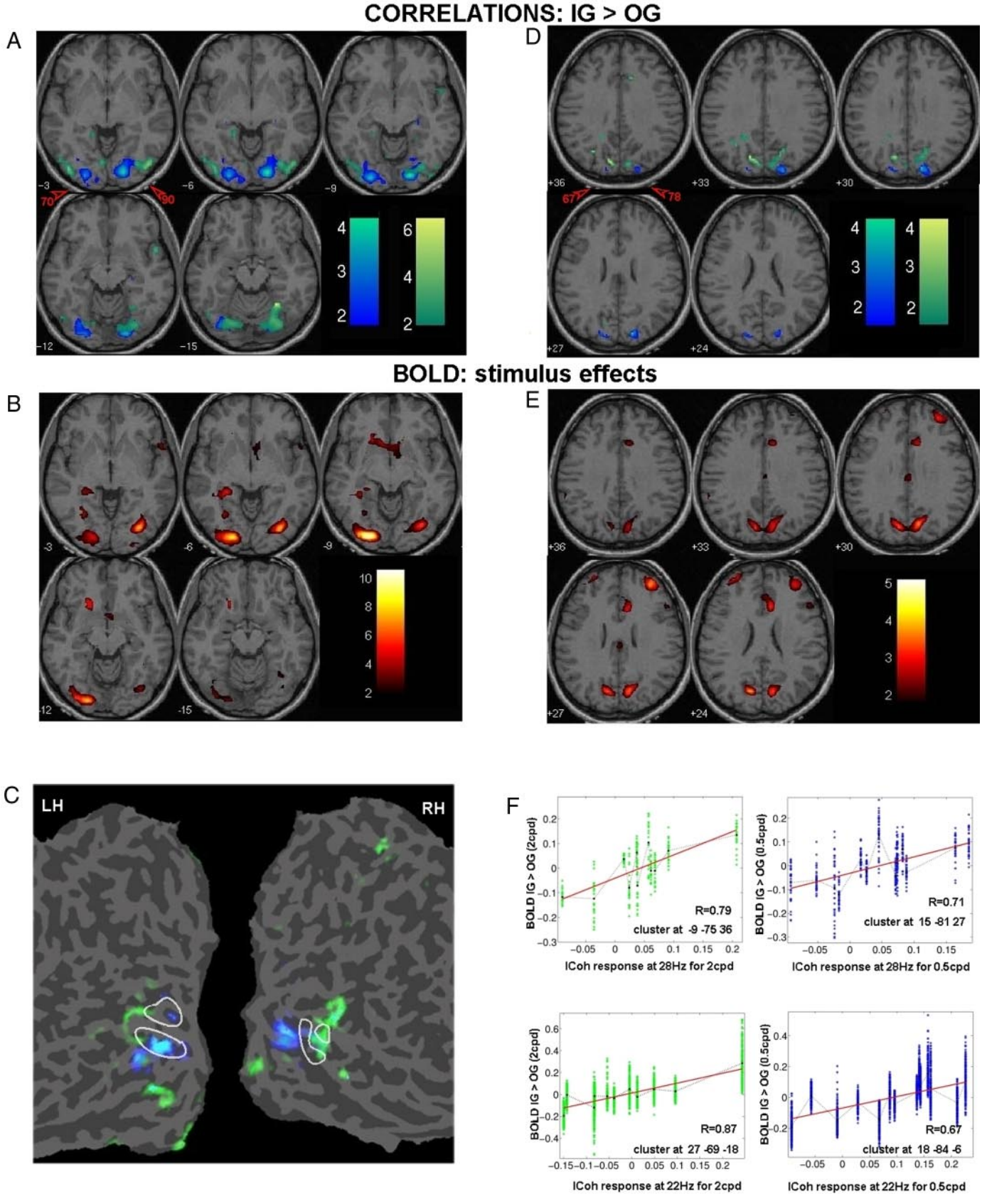

decrease in activation with an increase in SF, while dorsal locations revealed the opposite tendency.

Correlation analysis

The next step was to examine whether the ICoh and BOLD responses associated with interhemispheric interaction are related to each other. Correlation coefficients were computed between the ICoh and the BOLD responses for each voxel within an ROI. The ROI was defined as all the voxels activated with any one of the stimuli used (Fig. 6*A*).

To reveal the effects of interhemispheric interaction, we used the IG > OG contrast both in the EEG and BOLD data. The significant ICoh responses at the peak frequencies of beta1 and beta2 components (22 and 28 Hz) were correlated with the BOLD responses across subjects.

For each frequency of interest, the ICoh response was defined as the difference between ICoh values ($\sqrt{}$MSC, see METHODS) in the IG and OG conditions. The BOLD response was expressed as a BOLD contrast value (percentage signal change) between the same conditions. To render the fMRI and EEG data directly comparable with each other we averaged the BOLD responses to the two OG stimuli (OG-HR and OG-HL). The correlation was computed separately across SF conditions.

At the beta1 peak frequency, we used the ICoh responses from the 70–90 sensor pair as they were significant for both SF. As can be seen in Fig. 8, *A* and *C*, significant correlations converged into clusters within the ventral visual brain (collateral sulcus and fusiform gyrus bilaterally), where the relevant BOLD response was localized as well (Fig. 8*B*), with partial overlap.

The most salient ICoh responses at the beta2 peak frequency were obtained from sensor pairs 71–84 and 67–78. At 0.5 cpd, they correlated with BOLD in IPS (bilaterally) and, at 2.0 cpd, in the neighboring POF regions (Fig. 8*D*). The POF clusters partly covered dorsal locations, where we found the BOLD increase in the IG > OG contrast for the 2.0 cpd gratings (Fig. 8*E*). In the 0.5 cpd condition, this location was not significantly activated in the relevant contrast. As revealed by scatter plots (Fig. 8*F*), the correlations presented are not due to the outliers, but demonstrate a genuine ICoh/BOLD relationship.

In conclusion, the existence of significant positive correlations between stimulus-dependent increases in ICoh and BOLD indicates that the inter-hemispheric interactions revealed by the two methods are related to each other in specific cortical territories. In particular, we found that the high and low beta responses are related to separate locations, including ventral and dorsal extrastriate visual areas in the two hemispheres. The locations appeared to be replicable across SF. The clusters with significant BOLD response and clusters where the response was related to ICoh belonged to the same functional regions and partially overlapped.

DISCUSSION

The main findings in our study are as follows. First, the bilateral iso-oriented drifting gratings within the range of SF 0.5–4.0 cpd induced interhemispheric EEG coherence in the narrow bands peaking at 22 and 28 Hz. These peaks showed noncorrelated behavior across SF and distinct spatial distribution over the occipito-parietal brain regions. They differentiated the good-Gestalt stimulus (IG) from the bad-Gestalt stimulus (OG).

Second, the fMRI experiments revealed maximum BOLD response to the gratings at 0.5–2.0 cpd. Within this SF range the low-frequency gratings induced higher activation distributed in the striate and extrastriate areas. The interhemispheric integration (IG vs. OG or DG) increased BOLD in ventral and dorsal extrastriate locations. The BOLD response was partly invariant across SF (ventral clusters) and partly dependent on SF (ventral and dorsal clusters). The SF-conditioned part of the response decreased in ventral and increased in (medio-) dorsal locations as SF increased.

Third, the EEG coherence and fMRI BOLD integration-related responses were linearly coupled in certain extrastriate locations at both SF. The synchronization at different EEG frequencies correlated with BOLD in different areas. In particular, correlation maps for the low-beta ICoh response (22 Hz) converged in the ventral stream areas, partly overlapping clusters preferentially activated by the IG stimulus. The correlation maps at the high-beta frequencies (28 Hz) were located in the dorsal stream areas, partly overlapping with the BOLD response at 2 cpd.

Interhemispheric synchronization at various spatial frequencies

Here we confirmed our previous finding (Knyazeva et al. 2006) that coherent visual stimuli induce interhemispheric synchronization as opposed to the background or to the incoherent visual stimuli.

Furthermore, we demonstrated that the effect depends on the SF. To the best of our knowledge, interhemispheric synchronization has never been studied as a function of SF. Within the SF limits tested (0.25–8 cpd), for beta coherence we obtained significant effects in the range of 0.5–4.0 cpd. This SF range is consistent with maximum responses for the other measures of the activity of neuronal populations, including the BOLD

FIG. 8. The EEG coherence/BOLD correlation and activation maps for the group data. A: representative slices (*top*) show clusters with the BOLD response (IG > OG) proportional to the interhemispheric coherence from the 70–90 sensor pair for *beta1 frequency* (22 Hz). They are shown using the blue scale under low SF (LSF), and the green scale for medium SF (MSF) condition. Color bars show the significance of correlation coefficients expressed in *T* values. The centers of clusters are 27, −87, −9 (*right*) and −18, −84, −6 (*left*) for the LSF and 27, −69, −18 (right), and −24, −69, −18 (*left*) for MSF. For comparison, in the same data format, the main effect of Stimulus is superimposed on an individual brain (*B*). Color bars in *B* and *E* show *F* and *T* values, respectively, for BOLD (hot scale). *C*: same correlation maps as in *A* are superimposed on a single subject's flattened brain. White lines show the borders of the main effect of the stimulus. *D*: clusters with the BOLD response (IG > OG) proportional to the interhemispheric coherence from the 71–84 and 67–78 sensor pairs at the *beta2 frequency* (28 Hz). The blue scale represents the LSF, and the green one the MSF condition in *T* values of the significance of correlation coefficients. The centers of clusters for the LSF are 15, −81, 27 (*right*) and 18, −81, 27 (*left*) and for the MSF are 18, −69, 33 (*right*) and −9, −75, 36 (*left*). *E*: relevant activation (IG > OG contrast for the MSF stimuli) superposed on an individual brain is shown. *F*: scatterplots of individual BOLD responses are shown as a function of ICoh response for all the voxels in 4 clusters representing each statistical correlation map (4 maps: 2SF × 2 beta components, $P < 0.05$, corrected). Blue (for 0.5 cpd) and green (for 2.0 cpd) circles define the values for each voxel. The red arrows in *A* and *D* point to the EEG sensor markers.

response to sine-wave gratings (Singh et al. 2000), and the MEG power response in the gamma band to square-wave gratings (Adjamian et al. 2004).

The psychophysical research regarding interhemispheric interaction also provides corroborating evidence. In particular, the interhemispheric transfer of learning in the visual discrimination task occurred only for gratings with the fundamental SF not higher than 2 cpd (Berardi and Fiorentini 1987). These interactions were accompanied by the VEP changes that disappeared at SF beyond 4 cpd (Berardi et al. 1989).

Therefore within the range of SF studied, our evidence for interhemispheric synchronization agrees with the data from other domains. Most importantly, interhemispheric coherence might reflect the activity of the neural populations also involved in the special case of interhemispheric integration whose cognitive counterpart is interhemispheric transfer.

EEG beta band is a carrier of interhemispheric synchronization

We have found that in response to coherent stimuli, interhemispheric synchronization increases in the beta range. According to PCA, the synchronized activity could result from at least two noncorrelated pairs of sources producing narrowband signals. Their peak frequencies (22 and 28 Hz) agree with the human and animal evidence regarding intermediate distance synchronization. In humans, fronto-central interhemispheric synchronization in the 20- to 22-Hz range has been observed in MEG (Nikouline et al. 2001). Coherence between parietal and premotor areas increased at similar EEG frequencies (18–22 Hz) during the preparation of hand movements (Wheaton et al. 2005). Extrastriate intracranial signals synchronized in the 15- to 25-Hz range have been described by Tallon-Baudry and collaborators (2001). The precentral-postcentral synchronization in monkey brains was also carried out by narrow beta peaks at 20–23 and 29 Hz (Brovelli et al. 2004).

Notably, the beta-coherence peaks described in the literature may not correspond to the power peaks at the same frequency (Brovelli et al. 2004; Tallon-Baudry et al. 2001). Here, and in our previous work (Knyazeva et al. 2006), we reported similar phenomena. The coherence increase induced by collinear bilateral gratings was not accompanied by significant EEG power enhancement. This implies that the ICoh response resulted neither from volume conduction effects nor from myogenic artifacts, but emerged from true interhemispheric synchronization. The spatial and frequency selectivity of the response also confirms its authentic nature. Indeed if the interhemispheric synchrony was due to the passive spread of electric field, then the diffusion of synchrony would be observed within pairs of neighboring sensors (Lachaux et al. 1999). Were the myogenic component significant in our data, we could expect a broadband power increase (Goncharova et al. 2003) and correlated behavior across a wide spectral range including beta- and gamma-components (Thornton 1996). These effects are irreconcilable both with uncorrelated behavior of narrow beta sub-bands revealed here and with the significant increase in interhemispheric coherences accompanied by a decrease or no changes in the intrahemispheric occipito-temporal and parieto-temporal pairs (Fig. 2–4). The increase in interhemispheric synchronization of epidural EEG in animals (Kiper et al. 1999) (obtained with the same experimental paradigm as reported here) and the absence of interhemispheric effects with unilateral stimuli in humans (Knyazeva et al. 1999) also support the above arguments about the interhemispheric origin of ICoh increase.

The beta-band oscillations are widely recognized as a carrier of interhemispheric synchronization between sensorimotor areas (Chen et al. 2003; Gerloff et al. 1998; Nikouline et al. 2001; Serrien and Brown 2002). Our results show that this band mediates interhemispheric synchronization in the visual brain as well. Furthermore, there is direct evidence that extrastriate areas contribute to the processes of distant synchronization at beta frequencies. In intracranial recordings, sustained synchrony in the 15- to 25-Hz range has been observed between the fusiform gyrus and the lateral occipital sulcus during image rehearsal in short-term memory (Tallon-Baudry et al. 2001). Also the fusiform gyrus produces widespread beta-gamma synchronization with temporal, parietal, and frontal cortices in the face-recognition task (Klopp et al. 2000).

Taken together, the evidence suggests that the beta-band interhemispheric functions are not limited to a particular brain region or sensory modality. This inference is consistent with anatomical considerations (Aboitiz et al. 2003) and modeling results, which limit distant synchronization to the beta or lower frequencies, if conduction delays are >10 ms (Bibbig et al. 2002). The interhemispheric delays in humans are mostly between 10 and 15 ms (Aboitiz et al. 2003; Brown et al. 1994).

Factors behind the modulation of interhemispheric synchronization

The paradigm and stimuli similar to the ones we have chosen here have previously been studied in animal models (Castelo-Branco et al. 1998; Engel et al. 1991; Fries et al. 2001; Munk and Neuenschwander 2000; Nase et al. 2003) and tested in parallel animal and human experiments (Kiper et al. 1999; Knyazeva et al. 1999) and in humans with high-density EEG (Carmeli et al. 2005; Knyazeva et al. 2006). Our set of data has been analyzed with different methods including state-space analysis of synchronization (Carmeli et al. 2005), analysis of phase synchronization (Gysels and Knyazeva 2005), and analysis of the narrow band EEG coherence in Knyazeva et al. (2006) and in the present report.

As in the reports cited in the previous paragraph, we have found that synchronization increase is associated with the well-known trend of the visual system to group iso-oriented collinear patterns and to segment cross-oriented or noncollinear ones. Therefore the EEG coherence increase may be taken as a signature of interhemispheric integration in line with the hypothesis that synchronization provides a mechanism for transient associations between brain neuronal populations. In particular, the interplay between synchronization and desynchronization of the neuronal populations is thought to underlie feature grouping/segregation in object representation (Engel et al. 2001; Munk and Neuenschwander 2000; Singer 1999; Tallon-Baudry 2003; Varela et al. 2001).

It must be noticed that the statistically significant ICoh increase at a group level resulted from the individual responses that appeared to be stable over time. We have shown previously that the individual characteristics of the ICoh response

including spatial distribution and EEG frequency are reproducible months and even years after the initial experiments[3]. Therefore they might reflect true heterogeneity within the various brain mechanisms. Because the analysis of ICoh/BOLD relationships central to this study was based on the group data, the sources of between-subject variability in interhemispheric synchronization are of particular interest.

A possible cause of the between-subject variations could be a diversity of the cortico-cortical assemblies underlying the processes of grouping and segmentation. The *trans*-hemispheric assemblies are formed with long-range callosal connections. Highly arborized callosal axons allow synchronous excitation of multiple targets in the opposite hemisphere due to a single callosal neuron firing (Innocenti et al. 1994). Synaptic facilitation after the CC stimulation with pulse trains at the frequencies of ingenious brain rhythms (Cisse et al. 2004) suggests that the CC sustains interhemispheric synchronization. Indeed, callosal input was shown to be crucial for interhemispheric EEG synchronization by the studies in acallosal and split-brain humans (Knyazeva et al. 1997; Koeda et al. 1995; TenHouten et al. 1987). In normal subjects, event-related EEG coherence in the beta band was reported to be a function of the CC size (Stancak et al. 2002). Therefore variations in the CC morphology impact the individual differences in ICoh responses. The evidence for such "callosal fingerprints" has been documented both for monkeys (Van Essen et al. 1982) and for humans (Aboitiz et al. 1992; Baird et al. 2005; Byne et al. 1988).

Our preliminary data show that, indeed, the CC characteristics (regional myelination) might provide a significant impact (Fornari et al. 2004). However, co-factors involved in the synchronization response require further exploration.

BOLD response to visual stimuli at various spatial frequencies

MAIN EFFECT OF SPATIAL FREQUENCY. The BOLD responses to our stimuli clearly decreased with SF in the V1, V2, V3, and VP locations (Fig. 6). This is in agreement with other fMRI reports. Singh and collaborators, who studied spatial frequency tuning between 0.4 and 7 cpd, observed the peak BOLD response at 0.4 cpd in V2 and V3 areas (Singh et al. 2000). In V1, their tuning curves dropped between 4 and 7 cpd. Similarly, Huang and collaborators (2003) have shown a maximum BOLD increase in V1 for gratings at SF $\leq$3 cpd with a peak at $\sim$1 cpd. On the other hand, the responses in VP and V4 appeared to be stable within this range of spatial frequencies (Singh et al. 2000)

The location of the main SF effect (Fig. 6) is remarkably similar to the maps of preferred SF presented in the literature (e.g., in Tootell et al. 1988) and suggests that the activation induced by the high-frequency gratings attenuates with eccentricity. This may result from the fact that in the primate visual cortex, HSF-tuned striate neurons are observed only in the central projection area, whereas LSF-tuned cells are distributed across the whole striate cortex (Tootell et al. 1982, 1998).

INTERHEMISPHERIC INTEGRATION EFFECTS. ANOVA revealed greater BOLD responses to the good-Gestalt stimulus (IG) than to the bad-Gestalt stimuli (OG, DG) in the ventral stream areas surrounding the collateral sulcus and in the mediodorsal locations (POF, IPS) of both hemispheres. In the ventral locations, BOLD response was invariant across SF in some voxels and decreased with an increase in SF in the other voxels. These two types of responses were intermingled within the same territory confined to the LG/FFG, IOS, and LOS. Because of limited spatial resolution and group analysis of the data, it is difficult to figure out the SF tuning properties of a network or networks behind this ventral activation pattern. Yet taking into account mediodorsal locations that responded only to the MSF, we did show distributed networks associated with interhemispheric integration at different SF.

Another intriguing feature of the interhemispheric integration effect was the prevalence of right hemisphere responses to the LSF and of the left hemisphere to the MSF (Fig. 7, *C* and *D*). Distinct locations of the Stimulus versus SF effect suggest that the integrative circuits per se could be tuned to higher SF in the left hemisphere. This could partially explain the greater left hemisphere sensitivity to higher SF reported previously for various categories of objects/images (Iidaka et al. 2004; Kitterle et al. 1993; Peterzell et al. 1989; Whitman and Keegan 1991).

Therefore even with a rather limited range of SF, we have found discrete neural assemblies with different SF preferences. The greater response to the LSF suggests a higher sensitivity to global image attributes in the ventral object-processing areas, whereas salient activation in the mediodorsal networks in response to MSF points to the function of these networks—integrating detailed information.

Correlation maps suggest multi-site integration at different spatial frequencies

The linear relationship of local field potential (LFP) with BOLD has been revealed in monkeys (Logothetis et al. 2001) and, with hemodynamic response, in cats (Niessing et al. 2005). Importantly, correlations in cats had the LFP-frequency-specific character, being negative in the delta band and positive in the gamma-band. Because EEG corresponds to a sum of local field potentials, these experiments suggest that similar relationships could be expected between human EEG and BOLD responses (Menon and Crottaz-Herbette 2005). Indeed, several groups recently reported correlations between BOLD and EEG power (Goldman et al. 2002; Laufs et al. 2003; Liebenthal et al. 2003; Mukamel et al. 2005). These correlations have EEG-frequency-specific character. For instance, narrow beta-bands 17–23 and 24–30 Hz were shown to fluctuate in concert with BOLD in separate cortical regions (Laufs et al. 2003), similarly to independent behavior within the beta band revealed here. Yet our results go beyond that because they demonstrate the dynamics of synchronization not of power as in previous studies. It should be noted that interpretation of LFP power as the synchronization index in animal models (Niessing et al. 2005) is justified by known topography, whereas, in human noninvasive studies, the relationships between scalp EEG power and synchronization are much more uncertain because of the complicated three-dimensional structure of the brain (Nunez and Silberstein 2000). This motivated us to analyze the relationships between EEG coherence and fMRI BOLD signal.

[3] Some of the subjects involved in these experiments participated also in the series reported several years ago (Knyazeva et al. 1999).

Although correlation analysis as such does not provide any clues for causality, its interpretation requires certain assumptions with respect to cause-effect relationships. According to current views, synchronization might change neuronal population activity, thus leading to the BOLD modulation. In so doing, the networks generating synchronized EEG and BOLD signals may or may not overlap. In the first case, synchronization affects population activity in the same area, probably through recurrent connections in the local circuits, or else reciprocally, as in the situation of interhemispheric interactions.

Another possibility is that the synchronized output signal emerges at no visible activation cost (e.g., due to resetting activity/oscillations without a significant increase in firing rates) (Jackson et al. 2002; Rizzuto et al. 2003; Salazar et al. 2004). According to theoretical predictions and modeling studies (Bibbig et al. 2002; Chawla et al. 1999; Singer and Gray 1995), such a signal might more efficiently activate areas downstream or upstream in the same hemisphere or interhemispherically.[4] Experimental confirmation of the second scenario has been obtained by Salazar and collaborators (2004). The minimum assumption that fits both scenarios is that the correlations indicate areas where activation is sensitive to synchronization. Positive correlations, in particular, chart the areas where synchronization boosts activation—that is, recruits these areas for a dynamic functional network.

Therefore we have identified discrete regions where activation was sensitive and proportional to interhemispheric synchronization, in the ventral and dorsal extrastriate visual cortices. The clusters appeared to be bilateral but only partly symmetrical as might be expected from the mixed homotopic/heterotopic character of callosal connections (Innocenti 1986) as well as from the dissimilarity of the sulci/gyri configuration between the hemispheres.

The ventral activations correlated with the low-beta coherence at both SF. The MSF locations were more lateral and anterior than the LSF locations (Fig. 8*C*). The LSF clusters were mostly in the sulci (collateral, inferior occipital), whereas the MSF clusters occupied the gyri (fusiform, middle occipital), spreading to the lateral occipital cortex. The area where these two maps meet or overlap appeared to be the area of the BOLD main effect. Therefore our evidence suggests that the ventral networks involved in the interhemispheric integration are SF tuned and distributed. Recently, Gauthier with collaborators (2005) came to a similar conclusion on the independent processing of various SF in the fusiform area based on noncorrelated individual differences between the activations induced by LSF- versus HSF-filtered images.

In mediodorsal locations (POF/IPS), the high-beta correlations gave rise to the bilaterally symmetric clusters. The LSF correlation map occupied the posterior and inferior part of IPS, within the V7 boundaries, whereas the MSF correlation map represented a subregion of the POF abutting the superomedial margin of the same area. Therefore the networks involved in interhemispheric integration at both SF were distributed within the ventral and dorsal visual brain. This is consistent with the anatomy of visual connections that does not imply a single "terminal" (integrator) area (Bartels and Zeki 1998) and with the multiple levels of interhemispheric integration shown in other imaging experiments (Iacoboni and Zaidel 2004).

The analysis of centrally presented objects includes interhemispheric integration as a necessary step (Mima et al. 2001). In this connection, it is interesting to compare our locations with the so-called object-related circuits. All the areas identified here by correlation maps are known to be involved in the ventral or dorsal networks that respond when the subject is viewing coherent images/scenes against noise or scrambled images (Altmann et al. 2003; Avidan et al. 2003; Braddick et al. 2000; Epstein and Kanwisher 1998; Haxby et al. 2001; Ishai et al. 1999; Kourtzi et al. 2003). In particular, our ventral locations include the lateral-occipital complex, which implements grouping processes (Kourtzi and Kanwisher 2000; Mendola et al. 1999) and the convergence of different visual features (Grill-Spector 1997; Kourtzi and Kanwisher 2000).

Currently there is a debate as to the basic principles of object representation (for review, see Grill-Spector (2003). Malach and collaborators proposed that object-specific spatial resolution requirements are behind the organization of cortical representations (Malach et al. 2002). Although experimental testing of this idea requires a much wider SF range than that used in our experiments, our evidence suggests that the spatial scale of image analysis is among the factors contributing to distributed object representations.

[4] In our case, synchronized input supposedly comes from the opposite hemisphere. Due to the fact that callosal connections are reciprocal, each of the two interacting areas may be at the same time a source and a target of synchronization. However, this does not preclude synchronization at the lower/higher levels of the processing stream from being a co-factor.

ACKNOWLEDGMENTS

We thank Prof. G. M. Innocenti for helpful comments and valuable suggestions, and D. Polzik for assistance in the preparation of the manuscript. We are grateful to our peer-reviewers for meaningful comments on the manuscript.

GRANTS

This work was supported by Swiss National Science Foundation Grants 31–63894.00 and 3100A0-103993/1.

REFERENCES

Aboitiz F, Lopez J, and Montiel J. Long distance communication in the human brain: timing constraints for inter-hemispheric synchrony and the origin of brain lateralization. *Biol Res* 36: 89–99, 2003.

Aboitiz F, Scheibel AB, Fisher RS, and Zaidel E. Individual differences in brain asymmetries and fiber composition in the human corpus callosum. *Brain Res* 598: 154–161, 1992.

Adjamian P, Holliday IE, Barnes GR, Hillebrand A, Hadjipapas A, and Singh KD. Induced visual illusions and gamma oscillations in human primary visual cortex. *Eur J Neurosci* 20: 587–592, 2004.

Altmann CF, Bulthoff HH, and Kourtzi Z. Perceptual organization of local elements into global shapes in the human visual cortex. *Curr Biol* 13: 342–349, 2003.

Arruda JE, Weiler MD, Valentino D, Willis WG, Rossi JS, Stern RA, Gold SM, and Costa L. A guide for applying principal-components analysis and confirmatory factor analysis to quantitative electroencephalogram data. *Int J Psychophysiol* 23: 63–81, 1996.

Avidan G, Levy I, Hendler T, Zohary E, and Malach R. Spatial vs. object specific attention in high-order visual areas. *Neuroimage* 19: 308–318, 2003.

Bair W. Visual receptive field organization. *Curr Opin Neurobiol* 15: 459–464, 2005.

Baird AA, Colvin MK, Vanhorn JD, Inati S, and Gazzaniga MS. Functional connectivity: integrating behavioral, diffusion tensor imaging, and functional magnetic resonance imaging data sets. *J Cogn Neurosci* 17: 687–693, 2005.

Bandettini PA and Ungerleider LG. From neuron to BOLD: new connections. *Nat Neurosci* 4: 864–866, 2001.

Bartels A and Zeki S. The theory of multistage integration in the visual brain. *Proc Biol Sci* 265: 2327–2332, 1998.

Berardi N, Bodis-Wollner I, Fiorentini A, Giuffre G, and Morelli M. Electrophysiological evidence for interhemispheric transmission of visual information in man. *J Physiol* 411: 207–225, 1989.

Berardi N and Fiorentini A. Interhemispheric transfer of visual information in humans: spatial characteristics. *J Physiol* 384: 633–647, 1987.

Bertrand O and Tallon-Baudry C. Oscillatory gamma activity in humans: a possible role for object representation. *Int J Psychophysiol* 38: 211–223, 2000.

Bibbig A, Traub RD, and Whittington MA. Long-range synchronization of gamma and beta oscillations and the plasticity of excitatory and inhibitory synapses: a network model. *J Neurophysiol* 88: 1634–1654, 2002.

Boynton GM. Attention and visual perception. *Curr Opin Neurobiol* 15: 465–469, 2005.

Boynton GM, Engel SA, Glover GH, and Heeger DJ. Linear systems analysis of functional magnetic resonance imaging in human V1. *J Neurosci* 16: 4207–4221, 1996.

Braddick OJ, O'Brien JM, Wattam-Bell J, Atkinson J, and Turner R. Form and motion coherence activate independent, but not dorsal/ventral segregated, networks in the human brain. *Curr Biol* 10: 731–734, 2000.

Bressler SL. Large-scale cortical networks and cognition. *Brain Res Brain Res Rev* 20: 288–304, 1995.

Brovelli A, Ding M, Ledberg A, Chen Y, Nakamura R, and Bressler SL. Beta oscillations in a large-scale sensorimotor cortical network: directional influences revealed by Granger causality. *Proc Natl Acad Sci USA* 101: 9849–9854, 2004.

Brown WS, Larson EB, and Jeeves MA. Directional asymmetries in interhemispheric transmission time: evidence from visual evoked potentials. *Neuropsychologia* 32: 439–448, 1994.

Byne W, Bleier R, and Houston L. Variations in human corpus callosum do not predict gender: a study using magnetic resonance imaging. *Behav Neurosci* 102: 222–227, 1988.

Campbell FW and Robson JG. Application of Fourier analysis to the visibility of gratings. *J Physiol* 197: 551–566, 1968.

Carmeli C, Knyazeva MG, Innocenti GM, and De Feo O. Assessment of EEG synchronization based on state-space analysis. *Neuroimage* 25: 339–354, 2005.

Castelo-Branco M, Neuenschwander S, and Singer W. Synchronization of visual responses between the cortex, lateral geniculate nucleus, and retina in the anesthetized cat. *J Neurosci* 18: 6395–6410, 1998.

Chawla D, Lumer ED, and Friston KJ. The relationship between synchronization among neuronal populations and their mean activity levels. *Neural Comput* 11: 1389–1411, 1999.

Chen Y, Ding M, and Kelso JA. Task-related power and coherence changes in neuromagnetic activity during visuomotor coordination. *Exp Brain Res* 148: 105–116, 2003.

Cisse Y, Crochet S, Timofeev I, and Steriade M. Synaptic enhancement induced through callosal pathways in cat association cortex. *J Neurophysiol* 92: 3221–3232, 2004.

Curby K, Schyns P, Gosselin F, and Gauthier I. Differential use of spatial frequency scales for face recognition in a person with Asperger's syndrome (Abstract). *J Vision* 3: 821a, 2003.

Dakin SC and Bex PJ. Local and global visual grouping: tuning for spatial frequency and contrast. *J Vision* 1: 99–111, 2001.

Dale AM, Fischl B, and Sereno MI. Cortical surface-based analysis. I. Segmentation and surface reconstruction. *Neuroimage* 9: 179–194, 1999.

De Valois R and De Valois K. *Spatial Vision.* New York: Oxford Univ. Press, 1990.

Eckhorn R. Oscillatory and non-oscillatory synchronizations in the visual cortex and their possible roles in associations of visual features. *Prog Brain Res* 102: 405–426, 1994.

Eger E, Schyns PG, and Kleinschmidt A. Scale invariant adaptation in fusiform face-responsive regions. *Neuroimage* 22: 232–242, 2004.

Engel AK, Fries P, and Singer W. Dynamic predictions: oscillations and synchrony in top-down processing. *Nat Rev Neurosci* 2: 704–716, 2001.

Engel AK, Konig P, Kreiter AK, and Singer W. Interhemispheric synchronization of oscillatory neuronal responses in cat visual cortex. *Science* 252: 1177–1179, 1991.

Epstein R and Kanwisher N. A cortical representation of the local visual environment. *Nature* 392: 598–601, 1998.

Ferree TC. *Calculation of Average Reference.* Electrical Geodesics. Technical Note. Eugene, OR, 2000.

Fischl B, Sereno MI, and Dale AM. Cortical surface-based analysis. II. Inflation, flattening, and a surface-based coordinate system. *Neuroimage* 9: 195–207, 1999.

Fornari E, Knyazeva M, Martuzzi R, Meuli R, and Maeder P. *Visual spatial integration in children and adults: a combined fMRI/MTI study.* Society for Neuroscience 34th Annual Meeting, San Diego. Session 713.9, 2004.

Fries P. A mechanism for cognitive dynamics: neuronal communication through neuronal coherence. *Trends Cogn Sci* 9: 474–80, 2005.

Fries P, Neuenschwander S, Engel AK, Goebel R, and Singer W. Rapid feature selective neuronal synchronization through correlated latency shifting. *Nat Neurosci* 4: 194–200, 2001.

Friston KJ, Mechelli A, Turner R, and Price CJ. Nonlinear responses in fMRI: the Balloon model, Volterra kernels, and other hemodynamics. *Neuroimage* 12: 466–477, 2000.

Friston KJ, Worsley KJ, Frackowiak RSJ, Mazziotta JC, and Evans AC. Assessing the significance of focal activations using their spatial extent. *Hum Brain Mapp* 1: 210–220, 1993.

Gauthier I, Curby K, and Skudlarski P. Individual differences in FFA activity suggest independent processing at different spatial scales. *J Cogn Affect Behav Neurosci* 5: 222–234, 2005.

Georgeson MA. Spatial frequency analysis in early visual processing. *Philos Trans R Soc Lond B Biol Sci* 290: 11–22, 1980.

Gerloff C, Richard J, Hadley J, Schulman AE, Honda M, and Hallett M. Functional coupling and regional activation of human cortical motor areas during simple, internally paced and externally paced finger movements. *Brain* 121: 1513–1531, 1998.

Goldman RI, Stern JM, Engel J Jr, and Cohen MS. Simultaneous EEG and fMRI of the alpha rhythm. *Neuroreport* 13: 2487–2492, 2002.

Goncharova II, McFarland DJ, Vaughan TM, and Wolpaw JR. EMG contamination of EEG: spectral and topographical characteristics. *Clin Neurophysiol* 114: 1580–1593, 2003.

Gray CM, Engel AK, König P, and Singer W. Mechanisms underlying the generation of neuronal oscillations in cat visual cortex. In: *Induced Rhythms in the Brain Basar*, edited by Basar E and Bullock TH. Boston, Basel, Berlin: Birkhäuser, 1992.

Grill-Spector K. Convergence of visual cues in the human lateral occipital complex (LO). *Soc Neurosci Abstr* 27: 8482. 1997.

Grill-Spector K. The neural basis of object perception. *Curr Opin Neurobiol* 13: 159–166, 2003.

Grill-Spector K, Kushnir T, Edelman S, Avidan G, Itzchak Y, and Malach R. Differential processing of objects under various viewing conditions in the human lateral occipital complex. *Neuron* 24: 187–203, 1999.

Gysels E and Knyazeva M. A strategy for EEG synchronization analysis. (Abstract). *Brain Topogr* 18: 131, 2005.

Halliday DM, Rosenberg JR, Amjad AM, Breeze P, Conway BA, and Farmer SF. A framework for the analysis of mixed time series/point process data–theory and application to the study of physiological tremor, single motor unit discharges and electromyograms. *Prog Biophys Mol Biol* 64: 237–278, 1995.

Haxby JV, Gobbini MI, Furey ML, Ishai A, Schouten JL, and Pietrini P. Distributed and overlapping representations of faces and objects in ventral temporal cortex. *Science* 293: 2425–2430, 2001.

Huang J, Cooper TG, Satana B, Kaufman DI, and Cao Y. Visual distortion provoked by a stimulus in migraine associated with hyperneuronal activity. *Headache* 43: 664–671, 2003.

Iacoboni M and Zaidel E. Interhemispheric visuo-motor integration in humans: the role of the superior parietal cortex. *Neuropsychologia* 42: 419–425, 2004.

Iidaka T, Yamashita K, Kashikura K, and Yonekura Y. Spatial frequency of visual image modulates neural responses in the temporo-occipital lobe. An investigation with event-related fMRI. *Brain Res Cogn Brain Res* 18: 196–204, 2004.

Innocenti GM. The general organization of callosal connections. *Cereb Cortex* 5: 291–353, 1986.

Innocenti GM, Lehmann P, and Houzel JC. Computational structure of visual callosal axons. *Eur J Neurosci* 6: 918–935, 1994.

Ishai A, Ungerleider LG, Martin A, Schouten JL, and Haxby JV. Distributed representation of objects in the human ventral visual pathway. *Proc Natl Acad Sci USA* 96: 9379–9384, 1999.

Issa NP, Trepel C, and Stryker MP. Spatial frequency maps in cat visual cortex. *J Neurosci* 20: 8504–8514, 2000.

Jackson A, Spinks RL, Freeman TC, Wolpert DM, and Lemon RN. Rhythm generation in monkey motor cortex explored using pyramidal tract stimulation. *J Physiol* 541: 685–699, 2002.

Kaiser H. An index of factorial simplicity. *Psychometrica* 39: 31–36, 1974.

Kayser C, Kim M, Ugurbil K, Kim DS, and Konig P. A comparison of hemodynamic and neural responses in cat visual cortex using complex stimuli. *Cereb Cortex* 14: 881–891, 2004.

Kiper DC, Knyazeva MG, Tettoni L, and Innocenti GM. Visual stimulus-dependent changes in interhemispheric EEG coherence in ferrets. *J Neurophysiol* 82: 3082–3094, 1999.

Kitterle FL, Christman S, and Conesa J. Hemispheric differences in the interference among components of compound gratings. *Percept Psychophys* 54: 785–793, 1993.

Klopp J, Marinkovic K, Chauvel P, Nenov V, and Halgren E. Early widespread cortical distribution of coherent fusiform face selective activity. *Hum Brain Mapp* 11: 286–293, 2000.

Knyazeva M, Koeda T, Njiokiktjien C, Jonkman EJ, Kurganskaya M, de Sonneville L, and Vildavsky V. EEG coherence changes during finger tapping in acallosal and normal children: a study of inter- and intrahemispheric connectivity. *Behav Brain Res* 89: 243–258, 1997.

Knyazeva MG, Fornari E, Meuli R, Innocenti G, and Maeder P. Imaging of a synchronous neuronal assembly in the human visual brain. *Neuroimage* 29: 593–604, 2006.

Knyazeva MG, Kiper DC, Vildavski VY, Despland PA, Maeder-Ingvar M, and Innocenti GM. Visual stimulus-dependent changes in interhemispheric EEG coherence in humans. *J Neurophysiol* 82: 3095–3107, 1999.

Koeda T, Knyazeva M, Njiokiktjien C, Jonkman EJ, De Sonneville L, and Vildavsky V. The EEG in acallosal children. Coherence values in the resting state: left hemisphere compensatory mechanism? *Electroencephalogr Clin Neurophysiol* 95: 397–407, 1995.

Kourtzi Z and Kanwisher N. Cortical regions involved in perceiving object shape. *J Neurosci* 20: 3310–3318, 2000.

Kourtzi Z, Tolias AS, Altmann CF, Augath M, and Logothetis NK. Integration of local features into global shapes: monkey and human FMRI studies. *Neuron* 37: 333–346, 2003.

Lachaux JP, Rodriguez E, Martinerie J, and Varela FJ. Measuring phase synchrony in brain signals. *Hum Brain Mapp* 8: 194–208, 1999.

Laufs H, Kleinschmidt A, Beyerle A, Eger E, Salek-Haddadi A, Preibisch C, and Krakow K. EEG-correlated fMRI of human alpha activity. *Neuroimage* 19: 1463–1476, 2003.

Liebenthal E, Ellingson ML, Spanaki MV, Prieto TE, Ropella KM, and Binder JR. Simultaneous ERP and fMRI of the auditory cortex in a passive oddball paradigm. *Neuroimage* 19: 1395–1404, 2003.

Loftus GR and Harley EM. How different spatial-frequency components contribute to visual information acquisition. *J Exp Psychol Hum Percept Perform* 30: 104–118, 2004.

Logothetis NK, Pauls J, Augath M, Trinath T, and Oeltermann A. Neurophysiological investigation of the basis of the fMRI signal. *Nature* 412: 150–157, 2001.

Malach R, Levy I, and Hasson U. The topography of high-order human object areas. *Trends Cogn Sci* 6: 176–184, 2002.

McKeefry DJ, Watson JD, Frackowiak RS, Fong K, and Zeki S. The activity in human areas V1/V2, V3, and V5 during the perception of coherent and incoherent motion. *Neuroimage* 5: 1–12, 1997.

McKeefry DJ, and Zeki S. The position and topography of the human colour centre as revealed by functional magnetic resonance imaging. *Brain* 120: 2229–2242, 1997.

Mendola JD, Dale AM, Fischl B, Liu AK, and Tootell RB. The representation of illusory and real contours in human cortical visual areas revealed by functional magnetic resonance imaging. *J Neurosci* 19: 8560–8572, 1999.

Menon V and Crottaz-Herbette S. Combined EEG and fMRI studies of human brain function. *Int Rev Neurobiol* 66: 291–321, 2005.

Mima T, Oluwatimilehin T, Hiraoka T, and Hallett M. Transient interhemispheric neuronal synchrony correlates with object recognition. *J Neurosci* 21: 3942–3948, 2001.

Morrison DJ and Schyns PG. Usage of spatial scales for the categorization of faces, objects, and scenes. *Psychon Bull Rev* 8: 454–469, 2001.

Mukamel R, Gelbard H, Arieli A, Hasson U, Fried I, and Malach R. Coupling between neuronal firing, field potentials, and FMRI in human auditory cortex. *Science* 309: 951–954, 2005.

Munk MH and Neuenschwander S. High-frequency oscillations (20 to 120 Hz) and their role in visual processing. *J Clin Neurophysiol* 17: 341–360, 2000.

Munk MH, Nowak LG, Nelson JI, and Bullier J. Structural basis of cortical synchronization. II. Effects of cortical lesions. *J Neurophysiol* 74: 2401–2414, 1995.

Nase G, Singer W, Monyer H, and Engel AK. Features of neuronal synchrony in mouse visual cortex. *J Neurophysiol* 90: 1115–1123, 2003.

Niessing J, Ebisch B, Schmidt KE, Niessing M, Singer W, and Galuske RA. Hemodynamic signals correlate tightly with synchronized gamma oscillations. *Science* 309: 948–951, 2005.

Nikouline VV, Linkenkaer-Hansen K, Huttunen J, and Ilmoniemi RJ. Interhemispheric phase synchrony and amplitude correlation of spontaneous beta oscillations in human subjects: a magnetoencephalographic study. *Neuroreport* 12: 2487–2491, 2001.

Nunez PL and Silberstein RB. On the relationship of synaptic activity to macroscopic measurements: does co-registration of EEG with fMRI make sense? *Brain Topogr* 13: 79–96, 2000.

Nunez PL, Silberstein RB, Shi Z, Carpenter MR, Srinivasan R, Tucker DM, Doran SM, Cadusch PJ, and Wijesinghe RS. EEG coherency. II. Experimental comparisons of multiple measures. *Clin Neurophysiol* 110: 469–486, 1999.

Nunez PL, Srinivasan R, Westdorp AF, Wijesinghe RS, Tucker DM, Silberstein RB, and Cadusch PJ. EEG coherency. I. Statistics, reference electrode, volume conduction, Laplacians, cortical imaging, and interpretation at multiple scales. *Electroencephalogr Clin Neurophysiol* 103: 499–515, 1997.

Pallant J. *SPSS Survival Manual.* Buckingham, UK: Open University Press, 2001.

Perrin F, Pernier J, Bertrand O, and Echallier JF. Spherical splines for scalp potential and current density mapping. *Electroencephalogr Clin Neurophysiol* 72: 184–187, 1989.

Peterzell DH, Harvey LO, Jr, and Hardyck CD. Spatial frequencies and the cerebral hemispheres: contrast sensitivity, visible persistence, and letter classification. *Percept Psychophys* 46: 443–455, 1989.

Picton TW, Dimitrijevic A, John MS, and Van Roon P. The use of phase in the detection of auditory steady-state responses. *Clin Neurophysiol* 112: 1698–1711, 2001.

Rizzuto DS, Madsen JR, Bromfield EB, Schulze-Bonhage A, Seelig D, Aschenbrenner-Scheibe R, and Kahana MJ. Reset of human neocortical oscillations during a working memory task. *Proc Natl Acad Sci USA* 100: 7931–7936, 2003.

Salazar RF, Kayser C, and Konig P. Effects of training on neuronal activity and interactions in primary and higher visual cortices in the alert cat. *J Neurosci* 24: 1627–1636, 2004.

Serrien DJ and Brown P. The functional role of interhemispheric synchronization in the control of bimanual timing tasks. *Exp Brain Res* 147: 268–272, 2002.

Singer W. Synchronization of cortical activity and its putative role in information processing and learning. *Annu Rev Physiol* 55: 349–74, 1993.

Singer W. Neuronal synchrony: a versatile code for the definition of relations? *Neuron* 24: 111–125, 1999.

Singer W and Gray CM. Visual feature integration and the temporal correlation hypothesis. *Annu Rev Neurosci* 18: 555–586, 1995.

Singh KD, Smith AT, and Greenlee MW. Spatiotemporal frequency and direction sensitivities of human visual areas measured using fMRI. *Neuroimage* 12: 550–564, 2000.

Srinivasan R, Nunez PL, and Silberstein RB. Spatial filtering and neocortical dynamics: estimates of EEG coherence. *IEEE Trans Biomed Eng* 45: 814–826, 1998.

Stancak A, Lucking CH, and Kristeva-Feige R. The size of corpus callosum and functional connectivities of cortical regions in finger and shoulder movements. *Brain Res Cogn Brain Res* 13: 61–74, 2002.

Tallon-Baudry C. Oscillatory synchrony and human visual cognition. *J Physiol Paris* 97: 355–363, 2003.

Tallon-Baudry C, Bertrand O, and Fischer C. Oscillatory synchrony between human extrastriate areas during visual short-term memory maintenance. *J Neurosci* 21: RC177, 2001.

TenHouten WD, Walter DO, Hoppe KD, and Bogen JE. Alexithymia and the split brain. V. EEG alpha-band interhemispheric coherence analysis. *Psychother Psychosom* 47: 1–10, 1987.

Thornton KH. On the nature of artifacting the qEEG. *J Neurotherapy* 1: 32–39, 1996.

Tootell RB, Hadjikhani N, Mendola J, Marrett S, and Dale AM. From retinotopy to recognition: fMRI in human visual cortex. *Trends Cogn Sci* 21: 174–182, 1998.

Tootell RB, Silverman MS, Hamilton SL, Switkes E, and De Valois RL. Functional anatomy of macaque striate cortex. V. Spatial frequency. *J Neurosci* 8: 1610–1624, 1988.

Tootell RB, Silverman MS, Switkes E, and De Valois RL. Deoxyglucose analysis of retinotopic organization in primate striate cortex. *Science* 218: 902–904, 1982.

Tucker DM. Spatial sampling of head electrical fields: the geodesic sensor net. *Electroencephalogr Clin Neurophysiol* 87: 154–163, 1993.

Van Essen DC, Newsome WT, and Bixby JL. The pattern of interhemispheric connections and its relationship to extrastriate visual areas in the macaque monkey. *J Neurosci* 2: 265–283, 1982.

Varela F, Lachaux JP, Rodriguez E, and Martinerie J. The brainweb: phase synchronization and large-scale integration. *Nat Rev Neurosci* 2: 229–239, 2001.

Velicer WF and Fava J-L. An evaluation of the effects of variable sampling on component, image and factor analysis. *Multivariate Behav Res* 22: 193–210, 1987.

Wheaton LA, Nolte G, Bohlhalter S, Fridman E, and Hallett M. Synchronization of parietal and premotor areas during preparation and execution of praxis hand movements. *Clin Neurophysiol* 116: 1382–1390, 2005.

Whitman RD and Keegan JF. Lateralization of facial processing: a spatial frequency model. *Int J Neurosci* 60: 177–185, 1991.

Wilkinson F, James T, Wilson H, Gati J, Menon R, and Goodale M. An fMRI study of the selective activation of human extrastriate form vision areas by radial and concentric gratings. *Curr Biol* 10: 1455–1458, 2000.

Wilson HR and Wilkinson F. Evolving concepts of spatial channels in vision: from independence to nonlinear interactions. *Perception* 26: 939–960, 1997.

Wilson HR and Wilkinson F. Spatial channels in vision and spatial pooling. In: *The Visual Neurosciences,* ed. by Chalupa LM and Werner JS. Cambridge, MA: MIT Press, 2002.

Winston JS, Vuilleumier P, and Dolan RJ. Effects of low-spatial frequency components of fearful faces on fusiform cortex activity. *Curr Biol* 13: 1824–1829, 2003.

Yao H and Dan Y. Synaptic learning rules, cortical circuits, and visual function. *Neuroscientist* 11: 206–216, 2005.

Zeki S. *Vision of the Brain.* Oxford, UK: Blackwell, 1993.